Dynamic hotspots in the Uba7 UFD direct UbcH8 recognition

Çağdaş Dağ[1,2,3,4,], Mahil Lambert[1,4], Alp E. Kazar[1], Kerem Kahraman[1], Oktay Göcenler[1], Woonghee Lee[5], Cansu D. Tozkoparan Ceylan[1], Frank Löhr[4], Jin Gon Shim[6], Arthur L. Haas[7], Volker Dötsch[5], Joshua J. Ziarek[6], Emine Sonay Elgin[3,*]*

[1]Nanofabrication and Nanocharacterization Center for Scientific and Technological Advanced Research (n[2]STAR), Koç University, İstanbul, Turkiye

[2]Koç University Isbank Center for Infectious Diseases (KUISCID), Koç University, Istanbul, Turkiye

[3] Department of Chemistry, College of Sciences, Muğla Sıtkı Koçman University, Muğla, 48000, Turkiye

[4]Centre for Biomolecular Magnetic Resonance, Institute for Biophysical Chemistry, Goethe-University of Frankfurt/Main, Germany

[5]Department of Chemistry, University of Colorado Denver, Denver, CO 80204, USA

[6]Department of Pharmacology, Feinberg School of Medicine, Northwestern University, 320 East Superior Avenue, Chicago, IL, 460611, USA

[7]Department of Biochemistry and Molecular Biology, LSUHSC-School of Medicine, 1901 Perdido Street, New Orleans, LA, 70112, USA

*Corresponding author: cdag@ku.edu.tr selgin@mu.edu.tr

Abstract

The ISGylation pathway, a key post-translational modification, plays a pivotal role in the innate immune response by covalently attaching ISG15 to target proteins. This cascade involves a series of enzymatic steps, including activation by the E1 enzyme Uba7, conjugation by the E2 enzyme UbcH8, and ligation by an E3 ligase. Central to this process is the ubiquitin-fold domain (UFD) of Uba7, which facilitates the transfer of ISG15 to UbcH8. However, the structural and mechanistic details of this interaction remain poorly understood. In this work, we present the solution NMR structure and functional analysis of the ubiquitin-fold domain of human Uba7, the E1 enzyme in the ISGylation cascade. Through detailed NMR titration experiments and mutational studies, we mapped the interaction surface of Uba7-UFD with UbcH8, identifying key residues and their contributions to the E1-E2 interaction. We found that Uba7-UFD is flexible in its free form; this flexibility is conserved across ubiquitin-like systems but shows a regional shift that may play an important role in correct E2 and Ubl selection. Chemical shift perturbation and mutational analysis further demonstrate the importance of specific residues, particularly Cys996, in maintaining UFD's structural integrity and binding capacity. Additionally, mutations designed to alter the flexibility and length of the loop region between UFD and UbcH8 show significant effects on binding, indicating that these regions are crucial for efficient E2 recruitment. These findings provide new insights into the mechanistic basis of E2 enzyme selection in ISGylation and underscore the functional relevance of dynamic structural transitions in E1-E2 complex formation.

Statement of Significance

ISGylation is a key ubiquitin-like modification pathway essential for antiviral defense, immune regulation, and protein quality control. However, the molecular principles that govern communication between the E1 and E2 enzymes in this pathway remain poorly defined. Here, we present the first NMR structure of the human Uba7 ubiquitin-fold domain (UFD) and its interaction with UbcH8. Our findings reveal how structural flexibility within the UFD is crucial for specific and efficient E2 recognition, providing fundamental insight into the dynamic mechanism of ISGylation and advancing our understanding of ubiquitin-like enzyme cascades relevant to cellular regulation and disease.

52 **Introduction**

53 ISGylation is a post translational modification (PTM) that results in the binding of interferon-
54 stimulated gene 15 (ISG15) to the target protein. ISG15 is a 15 kDa ubiquitin-like protein (Ubl)
55 containing two ubiquitin-like domains connected by a short linker peptide (Haas et al., 1987).
56 Expression of ISG15 is primarily induced by type I interferon (IFN α/β) signaling (Farrell et al.,
57 1979), through interactions between IFN regulatory factors (IRFs) and interferon-stimulated
58 response element (ISRE)-containing promoters (Sadler and Williams, 2018). Innate immune
59 response on a molecular level is generated via host pattern-recognition receptors and expression
60 of IFN-I through downstream signaling. In this regard, ISG15 expression coincides with initiation
61 of the innate immune response which serves as the first line of defense against pathogens. After
62 expression, ISG15 takes part in innate immune response either as an intracellular regulatory
63 protein or through ISGylation of primarily pathogen proteins (Zhang et al., 2021). In the context
64 of the innate immune response, effectiveness of ISGylation against pathogens varies between
65 species. For instance, ISGylation in mice is shown to be a highly effective antiviral mechanism for
66 inhibiting viral assembly slowing down pathogenesis (Durfee et al., 2010). ISGylation of viral
67 proteins also interferes with localization, host-viral protein interactions, and protease activity
68 thereby strengthening the antiviral response (Rahnefeld et al., 2014). Whereas in humans, inherited
69 ISG15 deficiency only results in susceptibility to mycobacterial, not viral diseases indicating
70 differing effectiveness against pathogens and possible differences in ISGylation pathway between
71 species (Bogunovic et al., 2012).

72 Similar to ubiquitin, ISG15 is also covalently attached via its C-terminal LRLRGG motif to a
73 lysine residue on the target protein through an analogous E1-E2-E3 enzymatic cascade
74 (Narasimhan, Potter and Haas, 1996). ISGylation enzymatic cascade includes an activating E1

75 enzyme (Uba7/Ube1L), a conjugating E2 enzyme (UbcH8), and an E3 ligase (HERC5) which their
76 expression is simultaneously induced with ISG15 through ISRE containing elements. ISGylation
77 begins with an ATP dependent reaction of sequential adenylation at the C-terminal motif
78 "LRLRGG" generating an AMP-ISG15 intermediate which forms a thioester bond with the
79 catalytic cysteine of the E1 activation enzyme, Uba7. In this step, active site cysteine half domains,
80 the first catalytic cysteine half-domain (FCCH) and the second catalytic cysteine half-domain
81 (SSCH) of the E1 form a thioester bond with the adenylated C-terminal glycine of ISG15. The
82 ubiquitin folding domain (UFD) of Uba7 functions as the recognizing agent of the E2 enzyme and
83 ISG15 where ISG15 is transferred to the catalytic cysteine of the E2 conjugating enzyme, UbcH8,
84 through a transthioesterification reaction. E2 functions as a bridge between the Uba7 (E1), and
85 HERC5 (E3), enzymes containing catalytic domain interaction sites of both E1 and E3. In the
86 subsequent reaction, ISG15 is transferred to the catalytic cysteine of E3 through another
87 transthioesterification reaction then ligated to a lysine residue of the target protein in a nonspecific
88 manner (Haas, 2007). Despite its similarities, ISGylation differs considerably from ubiquitylation
89 in terms of variability and prevalence in the cell. Unlike its counterpart, ISGylation cascade
90 contains only one set of E1-E2 enzymes and therefore regulation of ISGylation is further
91 influenced through intrinsic interactions between enzymes of the cascade in addition to external
92 pathways regulating the ISGylation.
93 As the cornerstone of Ub/Ubl conjugation pathways, E1 enzymes are responsible for initiating the
94 activation of the corresponding Ub/Ubl along with its transfer to the relevant E2 enzymes. This
95 crucial function helps to ensure the accuracy and reliability of Ub/Ubl-mediated conjugation
96 pathways (Capili and Lima 2007, Streich and Haas, 2010) highlighting the crucial role that E1
97 enzymes play in maintaining the integrity of ubiquitylation pathways. Previous studies have

managed to identify crystal structures of Ub E1 along with E1s for Ub-like modifiers (Ubls) such as SUMO and Nedd8 (Figure 1), both singularly and in complex states with their corresponding Ubls (Olsen and Lima, 2013; Huang et al., 2005, Lois and Lima, 2005). Structures of the SUMO E1 provide mechanistic insights into SUMO activation and E2 recruitment to E1. A discovery from these studies was the revealing of the multidomain structure inherent to canonical E1s. The domains include a pseudodimeric adenylation domain which plays a crucial role in Ubl activation, a Cys domain which contains the catalytic cysteine residue and a ubiquitin-fold domain (UFD) involved in the recruitment of E2 (Figure 1). To better contextualize the structural findings of the present study, we first conducted a comparative analysis of E1 enzyme ubiquitin-fold domains (UFDs) from several ubiquitin and ubiquitin-like (Ubl) modification systems (Figure 1). The aim of this figure is to illustrate that in most available crystal structures of free (apo) E1 enzymes, the E2-binding regions of the UFD domains lack interpretable electron density, indicating substantial conformational flexibility in these segments. This absence of density across multiple E1–UFD structures—including Uba1, Uba2, Uba3, and Uba6—suggests that these regions are inherently disordered or mobile in solution until they engage their cognate E2 enzymes. Such disorder-to-order transitions have been previously proposed to facilitate accurate E2 selection and dynamic repositioning of the catalytic domains during transthiolation. Our NMR-derived structure of the human Uba7-UFD (Figure 1K) provides complementary insight into this phenomenon by capturing the domain in its solution state, where flexibility is preserved rather than averaged out as in crystal lattices. In constructing Figure 1, we intentionally combined representative E1–UFD structures, both apo and complexed with E2 or Ubl partners, to highlight how the flexible β-grasp and loop regions adopt defined conformations upon complex formation.

120 Furthermore, these prior structural studies have unveiled the considerable conformational shifts
121 E1s undergo to execute their roles effectively. In light of conformational changes revealing the
122 UFD, a hidden E2 binding area on the E1 is exposed, assisting in facilitating contact between the
123 Ubl thioester and E2 (Olsen and Lima, 2013). Upon the Ubl thioester's transfer from E1 to E2, it
124 is proposed that the UFD reverts to its originally locked conformation. This switch aids in the
125 release of the E2-Ub thioester product through a spatial mechanism (Olsen and Lima, 2013).
126 Similarly, E1-E2 interaction during ISGylation marks a crucial regulatory step of the ISGylation
127 pathway however while considerable insights have been attained regarding the structural insights
128 into E1 activity, the specific process at the atomic level has yet to be determined of ISGylation
129 pathway. The importance of flexible regions and flexibility in protein-protein interactions has
130 become increasingly evident with the advancement of structural methods. In this context,
131 "disorder-to-order transition" in protein binding regions is being extensively studied using NMR
132 spectroscopy and plays a crucial role in elucidating protein-protein interactions (Jubb, Blundell
133 and Ascher, 2015). Specific mechanistic and interactive characteristics of ISGylation are still
134 poorly understood.
135 In this study, we explore the NMR structure of Uba7-UFD, interaction dynamics and the critical
136 role of the disorder-to-order transition within the E1-E2 complex of the ISGylation cascade at the
137 residual level using NMR spectroscopy. The structural flexibility observed for Uba7-UFD in the
138 unbound state is consistent with a general feature of E1 enzymes, in which localized dynamic
139 elements are maintained within an otherwise well-folded UFD scaffold to support productive E2
140 engagement. Upon interaction with UbcH8, the relaxation profiles indicate a redistribution of
141 backbone dynamics within the UFD—most prominently around the highlighted β2/β4 surface—
142 suggesting that E2 binding modulates pre-existing motional properties rather than invoking a

143 global conformational switch. Notably, while flexibility at the UFD–E2 interface appears
144 conserved across ubiquitin-like activation systems, the specific segments exhibiting the strongest
145 dynamic signatures show a measurable regional shift between different E1–E2 pairs, providing a
146 plausible mechanism for fine-tuning E2 specificity and ensuring efficient ISG15 transfer. Through
147 detailed NMR titration experiments, we mapped the extensive interaction surfaces between Uba7-
148 UFD and UbcH8, identifying over 30 residues involved in this dynamic binding process. The study
149 also highlighted the significance of electrostatic complementarities between the interacting regions
150 of Uba7-UFD and UbcH8, which contribute to their stable complex formation. Furthermore,
151 mutational analysis underscored the importance of key residues, such as cysteine 996, in
152 maintaining the structural integrity and binding capacity of Uba7-UFD. These findings provide
153 novel insights into the conformational plasticity of E1 enzymes and their regulatory role in
154 ISGylation, paving the way for a deeper understanding of this post-translational modification
155 process at the molecular level.

156 **Materials and Methods**

157 **Construction of Uba7-UFD expression plasmid**

158 The DNA sequence coding for Uba7-UFD (amino acid residues 903-1011) was amplified from
159 pGEX-full length HsUba7 by polymerase chain reaction (PCR). Taq polymerase (Thermo) and
160 primers 5' Uba7-UFD-BglII (5'-GCGCAGATCTCAGACGTTCCATCACCTG-3') and 3' Uba7-
161 UFD-HindIII 5'-GCGCAAGCTTACAGCTCATAGTGCAGAGG-3' were used in the reaction.
162 Amplified PCR product was cleaned up using Omega PCR clean-up kit and digested with BglII
163 and HindIII while the pQE30-GBI expression vector was digested with BamHI and HindIII. The
164 digested PCR product and plasmid ligated with T4 DNA ligase. Accuracy of the cloned gene was
165 confirmed by DNA sequencing (Macrogen, Korea) using reverse and forward pQE30 primers.

166 Recombinant pQE-30-GBI-Uba7-UFD plasmid transformed into the chemically competent
167 SG13009 expression strain of *E. coli* using heat shock.

168 **Site-Directed mutagenesis to Uba7-UFD**

169 For site-directed mutagenesis PCR reaction, Pfu polymerase was mixed with template pQE-GBI-
170 Ube1-UFD plasmid and forward and reverse primers containing the desired mutation. Primer
171 names and sequences used for mutations are given below.

172 *5′ C996A 5′ GTGCTAGAGCTGAGCGCTGAGGGTGACGACG 3′*

173 *3′ C996A 5′ CGTCGTCACCCTCAGCGCTCAGCTCTAGCAC 3′*

174 *5′ C996S 5′ GTGCTAGAGCTGAGCAGCGAGGGTGACGACG 3′*

175 *3′ C996S 5′ CGTCGTCACCCTCTCGGCTCAGCTCTAGCAC 3′*

176 *5′ A1004C 5′ GGGTGACGACGAGGACACTTGCTTCCCACCTCTGCACTATG 3′*

177 *3′ A1004C 5′ CATAGTGCAGAGGTGGGAAGCAAGTGTCCTCGTCGTCACCC 3′*

178 Once completed, PCR reaction mixture was incubated with 10 U DpnI restriction enzyme for 2
179 hours at 37 °C to digest the template plasmid. Resulting reaction mixture containing amplified
180 mutant plasmid was transformed into Novablue competent *E. coli* cells. The existence of the
181 desired mutation was confirmed by DNA sequencing. Plasmids containing target mutation were
182 selected and transformed into competent SG13009 (pREP4) *E. coli* cells. Plasmids encoding
183 mutant R944L and 998GGG proteins were purchased from GENSCRIPT.

184 **Expression of recombinant GBI-Uba7-UFD fusion protein in *E. Coli***

185 The freshly-streaked single colony of SG13009 strain of *E. coli* containing PQE30-GBI-Uba7-
186 UFD plasmid was inoculated in 10 mL Luria Broth (LB) media containing 150 µg/mL ampicillin
187 and 50 µg/mL kanamycin. Inoculated culture was grown overnight with shaking at 250 rpm at 37
188 °C. Next morning, 10 mL overnight culture was added to 1 L fresh LB media containing the same
189 concentrations of antibiotics and grown at 37 °C and 250 rpm until OD_{600} reached 0.8. The protein
190 expression was induced with 1 mM IPTG. After induction, cells were grown for 5 more hours at

191 37 °C. Cells were then centrifuged at 4500 x g for 25 minutes at 4 °C and stored at – 80 °C until
192 protein purification.

193 **Refolding and purification of fusion protein with affinity chromatography**

194 For purification of GBI-Uba7-UFD fusion protein, cell paste was resuspended in 30 mL Lysis
195 buffer containing 50 mM Tris (pH 7.5), 150 mM NaCl, 5 mM DTT and sonicated at 4 °C, then
196 centrifuged at 15000 x g for 60 minutes at 4 °C. Proteins in pellet and supernatant were checked
197 by SDS-PAGE and supernatant were discarded. Inclusion bodies in pellet were washed two times
198 with 50 mL 0.5% Triton X-100 in 50 mM Tris (pH 7.5), 150 mM NaCl to solubilize membranes
199 and membrane proteins and then centrifuged at 15000 x g for 60 minutes at 4 °C. Cleaned inclusion
200 bodies were solubilized in 100 mL denaturation buffer containing 7 M Guanidium-HCl, 50 mM
201 Tris, 150 mM NaCl, 10 mM DTT overnight with stirring at 20 °C. The next day, the mixture was
202 centrifuged at 15000 x g for 60 minutes at 15 °C to separate insoluble components from the
203 solution. Refolding of fusion protein was achieved by dialysis. For this, supernatant was
204 transferred into a dialysis membrane (MWCO value 3500) and dialyzed twice against 4 liters of
205 50 mM Tris, 150 mM NaCl, 10 mM DTT pH 7.5 buffer for 8 hours at 15 °C. After second dialysis,
206 precipitated components were removed by centrifugation at 15000 x g for 60 minutes at 15 °C.
207 Refolded fusion protein was purified by immobilized metal ion affinity (IMAC) chromatography
208 using a 5 mL HisTrap HP column (GE HealthSciences) precharged with nickel and attached on an
209 Akta Prime Plus protein purification system. The dialyzed sample was bound to a HisTrap HP
210 column at a flow rate of 3 mL/min. Unbound proteins were washed away with a buffer containing
211 50 mM Tris-HCl, 150 mM NaCl, 5 mM DTT, 20 mM imidazole pH 7.5 until the absorbance at
212 280 nm was below 10 mAbs. Elution of HisTagged fusion protein was achieved by linearly
213 increasing the amount of elution buffer (50 mM Tris, 150 mM NaCl, 5 mM DTT, 500 mM
214 Imidazole pH 7.5) from 0 to 100 % in 30 mL volume. All fractions were analyzed by SDS-PAGE

215 and those containing the purified GBI-Uba7-UFD fusion protein were pooled, concentrated and
216 desalted with 20 mM phosphate Buffer pH: 7.4 to 200 µM volume in a pressure concentrator
217 (Stirred cell, Amicon) using a membrane with 3500 Da MWCO.

218 **Isotopically labeled protein expression**

219 For 1 L of M9 minimal media 200 mL sterile 5x M9 salts lacking ^{15}N-NH_4Cl (64 g Na_2HPO_4
220 $7H_2O$, 15 g KH_2PO_4, 2.5 g NaCl), were diluted to 950 mL with dd H_2O. 1 g ^{15}N-NH_4Cl (dissolved
221 in 10 mL ddH_2O and filter sterilized), 2 mL sterile 1 M $MgSO_4$, 20 mL 20% filter sterilized glucose
222 (for double labeled protein samples 2 g/L ^{13}C glucose), and 0.1 mL sterile 1M $CaCl_2$ was added to
223 M9 salts and the volume was completed to 1 L with sterile ddH_2O. Media was then supplemented
224 with trace metals and vitamins.

225 Freshly transformed cells were used to inoculate 20 mL of LB media containing ampicillin and
226 kanamycin. Cultures were grown overnight at 37 °C, 250 rpm. Cells were pelleted the next day by
227 centrifugation at 1000 x g for 10 min at 4 °C, resuspended in 10 mL of M9 minimal media and
228 added to the 1L of either ^{15}N-labeled M9 culture for ^{15}N-labeled protein production or ^{15}N-^{13}C
229 labeled M9 culture for double-labeled protein production. Protein expression was carried out as
230 described above with the exception that after induction with 0.5 mM IPTG, cells were incubated
231 at 25 °C for 15 hours to allow for expression of target proteins. Cells were then harvested by
232 centrifugation at 4000 x g for 30 minutes. Cell paste was kept at -20 °C until further processing.

233 **NMR data collection**

234 2D ^{1}H-^{15}N HSQC, 3D HNCA, 3D SE HNCO, 3D SE HNCACB, 3D SE HN(CO)CA, 3D SE
235 CCONH, 3D SE HCCONH, 3D SE HBHACONH, 3D HNCACO, 3D SE HNCOCACB, 3D
236 HCCH-TOCSY 3D SE ^{15}N-NOESY-HSQC, 3D SE ^{13}C-NOESY-HSQC-aliphatics and 3D ^{13}C-
237 NOESY-HSQC-aromatics were performed at 20 ^{0}C on Bruker Avance II 600 MHz spectrometer

238 with a triple resonance z-axis gradient CryoProbe. All NMR samples were prepared in 20 mM
239 sodium phosphate, pH 7.4 containing 5-10% D_2O and 0.05% sodium azide.

240 **NMR data processing, analysis and structure calculation**

241 All multidimensional NMR datasets were processed using NMRPipe (Delaglio et al., 1995). Raw
242 free-induction decay (FID) data were subjected to zero-filling to at least twice the acquired
243 complex points, apodized with a shifted sine-bell window, and Fourier-transformed in both
244 dimensions. Phase and baseline corrections were applied manually. Processed spectra were
245 visualized and analyzed using XEASY and the POKY suite (Lee et al., 2021). Backbone and side-
246 chain resonance assignments were obtained from standard 3D triple-resonance experiments
247 (HNCA, HNCO, HNCACB, HN(CO)CA, CCONH, HCCONH, HBHACONH, HCCH-TOCSY,
248 15N-NOESY-HSQC, and 13C-NOESY-HSQC). Secondary-structure elements were identified
249 from chemical-shift indices using CSI and torsion-angle restraints derived with TALOS+ (Shen et
250 al., 2009). Inter-residue NOE distance restraints were extracted from NOESY spectra and
251 combined with dihedral-angle restraints for structure calculations in POKY/CNS. The final
252 ensemble of 20 lowest-energy conformers was refined against all experimental restraints and
253 validated using standard NMR structure-quality metrics (RMSD, Ramachandran, and NOE
254 statistics).

255 All NMR titration experiments and HSQC spectra were acquired using isotopically labeled protein
256 samples at a concentration of 200 μM. HSQC cross-peak movements were quantified as a
257 combined ^{1}H-^{15}N chemical shift perturbation calculated from $\Delta\delta AV = [(\Delta\delta\ ^{1}H*5)^2 + (\Delta\delta\ ^{15}N)^2]^{½}$
258 equation. The structure calculations were performed using POKY (Lee et al., 2021) programs on
259 a computer running the MacOS operating system.

260 **Docking Analysis**

261 The docking process in HADDOCK2.4 docking protocol (de Vries et al., 2010) is divided into
262 three stages. In the first stage, the proteins are treated as rigid bodies, and their interaction energy
263 is calculated for different orientations. The orientations with the lowest energy are then selected
264 for further refinement. In the second stage, simulated annealing is used to refine the interface
265 between the two proteins. Simulated annealing is a Monte Carlo method that allows the system to
266 escape from local energy minima. In the context of protein-protein docking, simulated annealing
267 allows the proteins to explore different conformations at the interface and identify the
268 conformation with the most favorable energy. In the final stage, the complex is immersed in
269 solvent to improve the energetics. The solvent molecules are explicitly included in the simulation,
270 and their interactions with the proteins are taken into account. This stage helps to refine the
271 structure of the complex and ensure that it is stable in a solvated environment. By combining these
272 three stages, HADDOCK2.4 outputs a prediction of the structure of protein-protein complex.

273 **NMR relaxation measurements**

274 Backbone dynamics of Uba7-UFD and UbcH8 were characterized using ^{15}N relaxation
275 experiments (T_1, T_2, and $\{^1H\}$-^{15}N heteronuclear NOE) to assess conformational flexibility and
276 dynamic changes upon complex formation. Relaxation measurements were performed for the free
277 ^{15}N-labeled Uba7-UFD and free ^{15}N-labeled UbcH8 under identical buffer conditions (20 mM
278 phosphate buffer, pH 7.4, 150 mM NaCl, 5 mM DTT, 5–10% D_2O).

279 Experiments for Uba7-UFD were carried out at 20 °C on a Bruker Avance III 900 MHz
280 spectrometer equipped with a triple-resonance cryogenic probe, while UbcH8 relaxation data were
281 acquired under identical conditions on a Bruker Avance II 600 MHz spectrometer.

282 Standard Bruker pulse sequences were used for all relaxation measurements. T_1 relaxation times
283 were obtained using eight relaxation delays (10, 50, 100, 200, 400, 600, 800, and 1000 ms), and

284 T_2 relaxation times were recorded using eight delays (10, 30, 50, 70, 90, 110, 130, and 150 ms).
285 $\{^1H\}$-^{15}N heteronuclear NOE spectra were collected with and without proton presaturation (3 s)
286 using identical acquisition parameters. All spectra were processed with NMRPipe and analyzed
287 using Bruker Dynamics Center software.
288
289 **Results**
290 **Backbone and side-chain resonance assignments of native human Uba7-UFD**
291 Uba7-UFD residues 903-1011 were recombinantly produced with an N-terminal GBI fusion in *E.*
292 *coli* cells and purified using Ni^{2+} affinity chromatography. Despite efforts to produce a soluble
293 construct, the GBI-Uba7-UFD expressed into inclusion bodies similar to our previous study with
294 Uba3-UFD (Elgin et al., 2012). The most effective approach to refold GBI-Uba7-UFD was
295 denaturation with 7 M guanidinium chloride and 5 mM DTT followed by dialysis into a solution
296 containing 50 mM Tris, 150 mM NaCl, 5 mM DTT, pH 7.5. Unfortunately, Uba7-UFD possessed
297 very low stability/solubility once the GBI solubility tag was removed resulting in precipitation
298 within ~4 h (data not shown). We next evaluated the possibility of using GBI-Uba7-UFD fusion
299 for NMR structure and binding studies. Comparison of 2D ^1H-^{15}N HSQC spectra for both the free
300 domain and the GBI fusion showed no detectable difference in the amide resonances
301 demonstrating the fusion does not affect the Uba7-UFD tertiary structure (Supp Fig. 1).
302 Comparison of ^1H-^{15}N HSQC spectra collected before (day 1) and after (day 9) a suite of 3D
303 assignment experiments reveals no significant time-dependent changes (Supp Fig. 2). Therefore,
304 GBI-Uba7-UFD was found to be suitable for further structure data collection and titration
305 experiments.
306 The chemical shift dispersion of [*U*-^{15}N]-GBI-Uba7-UFD amide resonances are consistent with a
307 well-folded protein (Fig. 2A); however, only 71 of the 100 expected backbone N-H resonances

308 were observed (109 total residues including eight prolines). These were assigned to residues 919-
309 1011 using a suite of conventional 3D triple-resonance spectra from which secondary structure
310 was predicted using TALOS+ (Shen et al., 2009) (Fig. 2A). A stretch of seven residues following
311 the third beta-strand were unassignable. The homologous region of the two E1 enzyme UFDs,
312 Uba3 and Uba2 (Wang et al., 2009; Elgin et al., 2012), were similarly unassigned due to low signal
313 intensity in 3D experiments which suggests these missing peaks result from inherent plasticity of
314 these regions (Fig. 2B).

315 **NMR Structure determination of Human Uba7-UFD**

316 The three-dimensional structure of the human Uba7-UFD was successfully determined using
317 multi-dimensional NMR spectroscopy (Fig. 2C). A total of 1616 unique NOE distance and 153
318 (phi/psi) dihedral angle constraints are used in the final structure calculations; refinement statistics
319 for the ensemble of 20 lowest energy conformers are shown in Table 1. The final ensemble
320 exhibited good convergence with an average pairwise root mean square deviation (RMSD) of 0.9
321 Å for backbone atoms and 1.4 Å for all heavy atoms. The secondary structure consists of three α-
322 helices and four β-strands arranged in a ubiquitin fold domain (Fig. 2B, 2C; Supp Fig. 4) consistent
323 with previously reported ubiquitin-like domains (Wang et al., 2010; Lv et at., 2018). After the
324 second β-strand, a partially folded intermediate third β-strand is present, with distinct loops located
325 before and after it. These loops and β-strand may play a role in the interaction with the E2 enzyme
326 in the ISGylation cascade, similar to the mechanism observed in ubiquitination (Lv et al., 2018).
327 The crystal structures of apo E1 enzymes (PDB:7ZH9, 6CWZ, 7PVB) lack electron density in
328 certain portions of the UFDs (Walden, Podgorski, and Schulman, 2003) (Figure 1). This is
329 consistent with NMR analyses that the UFDs contain intrinsically disordered regions in their free
330 form (Wang et al., 2009; Elgin et al., 2012) that adopt stable secondary structures upon E1-E2
331 complexation (Huang et al., 2005; Wang et al., 2010) (Figure 1). Comparison of NMR structures

332 of UFD's from Uba7 and Uba3 shows that Uba7-UFD NMR structure shows a well-folded second
333 alpha helix (Figure 2B-Uba7_960-968), which is largely unfolded in Uba3-UFD (Figure 2B-
334 Uba3_397-403) (PDB 2LQ7; Fig. 1J-K,2B). In contrast, the third beta strand of Uba7-UFD (Figure
335 2B-Uba7_950-960), which is well defined in Uba3-UFD (Figure 2B-Uba3_388-392), is relatively
336 flexible (Fig. 1H-K). In addition, the NMR-derived structure showed that the acidic loop region
337 located between the fourth and fifth beta strands also exhibits much greater flexibility compared
338 to the corresponding loop region in Uba3-UFD (Fig. 1H-K). Although the overall ubiquitin fold
339 structure is conserved in both Uba7- and Uba3-UFDs, NMR ensembles clearly demonstrate that
340 the location of conformational flexibility is quite unique to each domain.

341 **Chemical shift mapping reveals the Uba7-UbcH8 interface**

342 To test the hypothesis that E1-UFD conformational disorder plays a role in E2
343 binding/selection/specificity, we performed an NMR titration to map UbcH8 onto the Uba7-UFD
344 surface. ^{1}H-^{15}N HSQC spectra were collected on [*U*-^{15}N]-Uba7-UFD mixed with increasing
345 concentrations of unlabeled-UbcH8 in molar ratios of 1:0.25, 1:0.5, 1:1 and 1:1.75 (Supp Fig. 5).
346 Inspection of these spectra revealed a subset of peaks that were dose-dependently perturbed upon
347 addition of UbcH8 (Figure 3A); combined ^{1}H/^{15}N chemical shift changes were calculated and the
348 most perturbed residues were highlighted onto the Uba7-UFD structure (Figure 3B, 3C). UbcH8
349 binding surface of Uba7-UFD appears to be quite large, involving about 18 residues. Interestingly,
350 some of the peaks displaying the largest chemical shift perturbations upon addition of UbcH8 were
351 weaker in intensity compared to the average peak intensities in the spectrum of the free Uba7-
352 UFD. In fact, four peaks with pronounced chemical shift perturbations corresponded to those
353 residues in the unassigned fragments and were absent in 3D spectra. One of the simplest
354 explanations for the low intensity and absence in 3D spectra is that these residues may undergo
355 conformational exchange on the microsecond-millisecond timescale (Supp Fig. 6).

356 We next mapped the binding interface onto the UbcH8 surface by titrating increasing
357 concentrations of Uba7-UFD into [*U*-^{15}N]-UbcH8. Substantial chemical shift perturbations
358 clustered to the UbcH8 N-terminal region, helix 1, strands 1-3, and helix 3 (Figure 3D-F). Several
359 peaks were also noted to disappear in the N-terminal region, helix 1, strands 1-3, and helix 3 upon
360 addition of unlabeled Uba7-UFD (Supp Fig. 7). This result is consistent with the mutational study
361 showing that the N-terminal region of UbcH8 is important in Uba7 interaction (Huibregtse et al.
362 2008).

363 **NMR data driven docking of UbcH8 and Uba7-UFD complex**

364 Next, we used the most substantial CSPs from our NMR titrations on the isolated domain
365 interactions to restrain a model of the full-length Uba7-HFB/UbcH8 complex using the
366 HADDOCK 2.4 NMR-based docking protocol (Vries et al., 2010). The AlphaFold Uba7 model
367 (APSD: AF-P41226-F1-v4) and the UbcH8 crystal structure (PDB: 1WZV) were used as inputs
368 and the resulting cluster with the lowest HADDOCK score was analyzed (Figure 4). The
369 HADDOCK model illustrates how complexation is facilitated by two sets of charge-charge
370 interactions; specifically, Uba7-UFD ^{999}DDEDTA^{1003} and ^{950}SALLYAAGWSPEK^{962}
371 complement UbcH8 ^{5}MRVVKE^{10} and ^{25}LSSDD^{29}, respectively. Furthermore, a series of
372 hydrophobic and charged residues surrounding the active site cysteine undergoes conformational
373 changes during the transthiolation stage (Figure 4). The spatial arrangement of these regions
374 precisely orients UbcH8 to ensure efficient ISG transfer between catalytic cysteine residues. We
375 also collected relaxation datasets for the Uba7-UFD:UbcH8 complex at a 1:2 molar ratio; however,
376 several resonances disappeared upon complex formation, preventing reliable fitting of relaxation
377 curves and thus precluding publication-quality analysis.

378

379

380 **Dynamics of Uba7 UFD**

381 To characterize the internal motions and structural rigidity of the Uba7 UFD in solution, backbone
382 ^{15}N relaxation measurements were obtained, including longitudinal relaxation times (T_1),
383 transverse relaxation times (T_2), T_1/T_2 ratios, and $\{^1H\}$-^{15}N heteronuclear NOE values (Figure 5).
384 The overall relaxation profiles demonstrate that Uba7-UFD adopts a well-folded and dynamically
385 stable β-grasp architecture, with relaxation parameters typical for a compact monomeric protein
386 of this size (~11 kDa). Regions corresponding to the β2 (residues 944-951) and β4 (residues 984-
387 989) strands, which form the E2-binding surface are highlighted in orange. These segments show
388 slightly lower $\{^1H\}$-^{15}N NOE values and β2 segment show slightly higher T_2 relaxation times,
389 indicating enhanced local flexibility relative to the β-sheet core. Such mobility is often observed
390 in loop regions or solvent-exposed β-strand edges that mediate transient interactions. The loop
391 region spanning residues 996-1008 exhibits low $\{^1H\}$-^{15}N NOE values and prolonged T_2 relaxation
392 times, indicating enhanced backbone flexibility compared with the rest of the Uba7-UFD domain.
393 This flexible segment forms part of the surface that interacts with ISG15 and likely contributes to
394 its recognition. The observed mobility suggests that this loop can undergo transient conformational
395 adjustments, allowing optimal positioning of ISG15 during E1-E2-substrate transfer. Such
396 dynamic behavior may therefore play a crucial role in facilitating ISG15 conjugation and ensuring
397 efficient catalysis within the ISGylation pathway.

398 To assess how E2 recruitment reshapes UFD dynamics, equivalent relaxation measurements were
399 collected for ^{15}N-labeled Uba7-UFD in the presence of unlabeled UbcH8 (Figure 5E–H).
400 Consistent with complex formation, the relaxation behavior shifts toward values expected for a
401 higher effective molecular size, including increased T_1 and elevated T_1/T_2 ratios across the
402 observable residues (Figure 5E,G). At the same time, residue-specific heterogeneity becomes more

403 pronounced within the highlighted β2/β4 surface and adjacent segments, consistent with binding-
404 coupled changes in local mobility and/or conformational exchange at the interface (Figure 5F,H).
405 We note that complex formation can lead to the disappearance of a subset of resonances, which
406 limits quantitative analysis for all residues and is consistent with intermediate-timescale exchange
407 contributions in portions of the binding surface. The elevated mobility observed in β2/β4 and the
408 996–1008 loop provides a plausible physical basis for the disorder-to-order or adaptive-fit
409 behavior inferred from binding and structural analyses, helping to reconcile how Uba7-UFD can
410 remain stably folded while retaining the conformational plasticity required for efficient E2
411 recruitment and productive transthiolation during ISGylation.

412 Together, these data reveal that Uba7-UFD possesses a hierarchical dynamic profile, where
413 structural rigidity within the β-sheet framework coexists with localized flexibility at the potential
414 binding surface features likely critical for efficient recognition and alignment with its cognate E2
415 enzyme during ISGylation.
416

417 **Dynamics of E1 UFD binding surface on UbcH8**

418 The dynamical behavior of the UbcH8 was also probed using ^{15}N T1, ^{15}N T2, and {^{1}H}-^{15}N
419 heteronuclear NOE relaxation experiments (Lakomek, Ying and Bax, 2013). Figures 6A and 6B
420 show the T1 and T2 relaxation rates plotted against the residue number and color mapped on the
421 crystal structure of UbcH8 (PDB:1WZW), respectively. Residues with high T1 and low T2
422 relaxation rates corresponding to relatively rigid regions are colored in green whereas those
423 displaying lower T1 and higher T2 relaxation rate hence higher flexibility are shown in yellow,
424 orange, and red in the order of increasing flexibility. Gray color corresponds to the unassigned
425 region. Figure 6C shows the heteronuclear ^{15}N-^{1}H NOE values plotted as a function of UbcH8

426 amino acid sequence. Fitting of data was done with the help of Bruker dynamics center and which
427 showed more than 95% confidence level. All together, T1 and T2 relaxation rates and
428 heteronuclear NOE values measured for UbcH8 consistently show that while the core of the
429 protein is rigid, the outward-facing residues on the conserved N-terminal α-helix show enhanced
430 flexibility, consistent with their proposed role in the UbcH8-binding interface (Figure 6D). Our
431 docking studies show that this region of UbcH8 is directly involved in the interaction with Uba7-
432 UFD. This relatively higher mobility may contribute to the E2's interaction and function by
433 facilitating conformational changes necessary for E1–E2 transthiolation.
434
435 **Conformational Flexibility of Uba7-UFD and Its Role in E2 Binding: Insights from Mutational**
436 **Analysis**
437 NMR solution structure of free Uba7-UFD indicated that the putative E2 binding region might be
438 flexible and experiencing conformational plasticity, transitioning among multiple conformational
439 states. Comparably, conformational flexibility/heterogeneity has been observed in E2 binding
440 surfaces of SUMO (Wang et al., 2009) and Nedd8 E1 UFD (Elgin et al., 2012). Notably this
441 conformational flexibility has been shown to be functionally important in SUMO conjugation
442 (Wang et al., 2009).
443 To further explore this phenomenon, we designed and analyzed a series of mutants to determine
444 how these alterations would affect E2 binding to Uba7-UFD. Specifically, we aimed to identify
445 the role of individual amino acids in maintaining the structural integrity and interaction capabilities
446 of the UFD domain. Given the high degree of plasticity observed in the putative E2 binding region,
447 understanding how mutations influence this flexibility is crucial. This investigation not only
448 provides insight into the specific amino acid interactions that are critical for binding but also sheds
449 light on the overall mechanism by which Uba7-UFD achieves its conformational adaptability. By

450 mapping these interactions and comparing the behavior of wild-type and mutant proteins, we
451 sought to delineate the structural elements that enable effective binding and subsequent functional
452 outcomes.

453 **Role C996 in Uba7-UFD conformational integrity and UbcH8 binding**

454 In order to determine the effect of mutations on E2 binding to Uba7-UFD, seven mutants were
455 created and five of them also titrated with UbcH8. Full length Uba7 protein contains a total of 17
456 cysteine residues, only one of which is in the UFD. Since this domain does not contain any other
457 cysteine residue to form disulfide bridge with C996, this single cysteine probably remains reduced.
458 C996 is located in the end of the second beta sheet, and while the subsequent amino acids show a
459 very flexible behavior in the structure, cysteine and previous amino acids have formed a stable
460 beta sheet secondary structure form.

461 We first mutated the free cysteine to alanine, which is the most preferred amino acid in mutation
462 scans. Overlay of ^{1}H-^{15}N HSQC spectra of wild-type and C996A variant shows that the overall
463 conformations of the mutant and wild-type proteins remain largely the same (Supp Figure 9). In
464 contrast, changes in chemical shift values were observed around the mutated region, indicating a
465 systematic reorganization in the preceding and subsequent beta sheets (Figure 7A). Figure 7B
466 shows the residues affected by C996A mutation mapped onto the Uba7-UFD structure. Residues
467 with chemical shift perturbations larger than 0.4 and 0.2 ppm colored in orange and merigold,
468 respectively, are mostly clustered in neighboring B1, and B4 strands and alpha 1 helix. In order to
469 determine the effect of mutation on E2 binding to Uba7-UFD, mutant protein was titrated with
470 UbcH8. Supp Figure 10 shows the overlay of ^{1}H-^{15}N HSQC spectra of Uba7-UFD-C996A before
471 and after addition of various amounts of UbcH8. No significant ^{1}H-^{15}N chemical shift
472 perturbations in C996A mutant upon addition of UbcH8 was observed and addition of more and

473 more of UbcH8 resulted in disappearance of some of the peaks involved in binding. These titration
474 studies clearly indicate that C996 is important for Uba7-UFD-UbcH8 interaction (Supp Figure 10).
475 Mutation of C996 to alanine appeared to have effect on UbcH8 binding. Since mutation of cysteine
476 to alanine results in truncation of the side chain at the C-beta, the goal of C996S mutation was to
477 replace –SH group with –OH group to see if this would restore the UbcH8 binding. The
478 comparison of ^{1}H-^{15}N HSQC spectrum of C996S with that of wild-type shows that the overall
479 conformation of C996S mutant is very similar to that of wild-type (Supp Figure 11) and as in
480 C996A mutant, significant chemical shift perturbations are located around the mutation site
481 (Figure 7C-7D). NMR binding studies carried out using ^{15}N labeled Ubc7-UFD C996S further
482 confirmed the role of C996 in UbcH8 binding since there were no significant chemical shift
483 perturbations in the ^{1}H-^{15}N HSQC spectra of C996S mutant upon addition of UbcH8(Supp Figure
484 12). The failure of the -OH group in restoring the UbcH8 binding suggests that free -SH might not
485 merely be involved in hydrogen bonding but might be important in providing necessary flexibility
486 for UbcH8 interaction (Bhopatkar et al., 2020).
487 After determining that free cysteine was necessary for UbcH8 binding/for keeping Uba7-UFD in
488 a suitable conformation for the UbcH8 binding we searched for amino acids in close proximity to
489 C996 within Uba7-UFD to test the effect of breaking C996 intermolecular interactions on the
490 conformation of the domain as well as on UbcH8 binding. Amino acids directly interacting with
491 C996 were identified through NOE analysis. NOE peaks observed between C996 and R944
492 indicated that there is an interaction between these two amino acids. Therefore, an R944L mutant
493 protein was generated, produced, and purified after refolding. Gel filtration chromatography of
494 purified ^{15}N-GBI-Uba7-UFD resulted in two separate peaks with the same molecular weight
495 confirmed by SDS-PAGE analysis. Peaks were collected in separate fractions and analyzed by

496 NMR. ^{1}H-^{15}N HSQC spectra showed that the peak eluted first from the gel filtration
497 column was completely misfolded/aggregated (Supp Figure 13A) while the fraction
498 corresponding to the second peak consisted of a mixture of both folded and misfolded
499 fusion protein (Supp Figure 13B). Gel filtration chromatography and NMR results
500 clearly show that R944 and its interaction with C996 are important for conformational
501 stability of Uba7-UFD and mutation of R944 to alanine makes domain prominent to
502 aggregation. The role of free cysteine amino acid in protein structure and internal
503 dynamics is often overlooked. However, a study conducted by Mazmanian et al. in 2016
504 examined the participation and significance of free cysteine amino acids in hydrogen
505 bonding networks in detail (Mazmanian et al., 2016). In the case of the Uba7-UFD
506 complex, when a cysteine atom forms a hydrogen bond with arginine (R944), it exhibits
507 distinct interaction patterns depending on the charge of the hydrogen bond donor.
508 Specifically, cysteine forms shorter and more linear hydrogen bonds with positively
509 charged residues such as histidine (His^{+}), lysine (Lys^{+}), and arginine (Arg^{+}), where the
510 hydrogen–sulfur distance (H···S) is less than 2.5 Å, and the bond angle (N–H···S) exceeds
511 150° (Mazmanian et al., 2016). In contrast, hydrogen bonds with neutral donors are
512 longer (H···S > 2.5 Å) and less linear (N–H···S < 150°). Notably, Arg^{+} donates two
513 hydrogen bonds to the cysteine thiol (CysSH), a characteristic not observed in other
514 residues (Mazmanian et al., 2016). These findings align with previous studies
515 demonstrating that positively charged hydrogen bond donors preferentially form
516 stronger and more directional interactions with thiol groups, contributing to protein

517 stability and conformational flexibility. Thus, the Uba7-UFD complex exemplifies the
518 critical role of free cysteines in fine-tuning the stability and plasticity of protein
519 structures.
520
521 **Effect of acidic loop flexibility and length on Uba7-UFD interaction with UbcH8**
522 As mentioned above, our NMR solution structure of Uba7-UFD shows that the loop region that
523 comes right after the C996 is relatively flexible. Since this loop is involved in interaction with
524 UbcH8, one question is whether restricting this flexibility would prevent binding. To test this,
525 another mutant was designed aiming to form a disulfide bond between the single cysteine 996 and
526 alanine 1004. In this mutant, A1004 was individually replaced by cysteine. This variant was also
527 expressed as inclusion bodies, solubilized with 7M GdnHCl and refolded by dialysis as described
528 previously. Supp Figure 14 shows an overlay of ^{1}H-^{15}N HSQC spectra of A1004C mutant in the
529 absence and presence of various amounts of UbcH8. Figure 7E shows the chemical shift
530 perturbation analysis from the titration experiment. Unlike the previous mutations, this mutant
531 variant still showed intrinsically interacted with UbcH8. As seen in Figure 7F, the interaction
532 surface is also partially compatible with the interaction surface of the WT protein. Opposite to
533 WT, A1004C mutant's 1st beta sheet region did not show any interaction with UbcH8.
534 The acidic loop interacting with UbcH8 has been extended with a glycine amino acid as a final
535 mutation approach (998GGG). The 998GGG mutant protein has been produced, purified, and
536 subjected to ^{1}H-^{15}N HSQC spectrum collection. Although there were regional differences in the
537 obtained spectrum, no significant changes were observed in the overall distribution (Supp Figure
538 15A). Unlabeled UbcH8 has been added to the obtained protein in a 1:1 ratio. Upon examination
539 of the spectra obtained after mixing the apo form of 998GGG with UbcH8, no changes were

540 observed in the chemical shift values indicating that integrity of the loop was necessary for UbcH8
541 binding. (Supp Figure 15B).

542 **Discussion**

543 Ubiquitin and Ubiquitin-like post-translational modification systems are of great importance to
544 organisms due to their extensive regulatory roles within cells. Elucidating the mechanisms at the
545 atomic level within the enzymatic cascades that form the basis of Ub and Ubl post-translational
546 modification systems has been a significant topic in biochemistry and structural biology for
547 decades. Although the atomic-level details of the mechanisms of systems such as ubiquitination,
548 neddylation, and sumoylation have been examined, structural studies on the ISGylation system
549 were not available until recent years. Specifically, due to the high plasticity of the ubiquitin fold
550 domain of the E1 enzyme, determining its structure has taken a considerable amount of time.
551 During the preparation of our manuscript, two additional papers aimed at elucidating the details of
552 ISGylation have been published (Wallace et al., 2023; Afsar et al., 2023). Although Cryo-EM and
553 crystal structures are excellent tools for visualizing the overall mechanism of systems, they are
554 still static and frozen structures. This makes them less effective for examining weak interaction
555 surfaces and low-affinity complex structures. At this point, NMR spectroscopy continues to be an
556 important structural biology method, providing atomic-level information to complement the
557 remarkable findings from other methods and to elucidate the side effects caused by freezing. In
558 the first part of our study, we determined the NMR structure of the ISGylation E1 enzyme and
559 observed that the plasticity and unstable beta-sheet surfaces exhibited in solution are believed to
560 play a significant role in the system's operation and selectivity.

561 Contemporary Cryo-EM structures, especially those examining the E1-E2 interaction, present
562 differing results regarding the amino acids and interaction angles involved in the interaction

563 between the first alpha helix of the E2 enzyme and the high plasticity regions of the E1 UF domain
564 (Wallace et al., 2023; Afsar et al., 2023). Despite the high overall resolutions of these structures,
565 it is notable that the resolution in these domains sometimes drops regionally to 4-5 Å. The direct
566 interactions obtained from our NMR data-driven model show greater alignment with the findings
567 of Wallace et al. 2023.
568 Findings from T1 and T2 relaxation experiments, coupled with titration and docking data, provide
569 a coherent picture suggesting that the N terminus region of Ubch8 is more flexible and that this
570 flexibility is relevant to the interaction with the Uba7-UFD. NMR characterization studies of
571 Uba7-UFD variants showed that both wild type and mutant domains have a high tendency to
572 aggregate. None of the designed mutant Uba7-UFDs was more stable than the wild type Uba7-
573 UFD. Our NMR mapping study showed that UbcH8 binding surface of Uba7-UFD is substantial
574 and there are over 30 amino acids directly involved in binding. This study also showed that a single
575 reduced cysteine residue at position 996 may play a major role in domain stability and fine tuning
576 of plasticity.

577 **Conclusion**

578 Our study has reiterated the importance of examining protein structures and dynamics in solution.
579 It has been demonstrated that the UFD domain of the Uba7 protein undergoes conformational
580 changes upon binding to UbcH8, consistent with the induced fit model. Structural analysis of the
581 Uba7 UFD and complex structures obtained from other systems have shown that a large surface
582 area of the UFD interacts with E2, highlighting the significance of this interaction in E1-E2 binding
583 and proper E2 selection. Additionally, structural investigations have revealed that a region on the
584 E1 UFD interacts with Ubiquitin/Ubiquitin-like proteins. It is important to conduct new studies to
585 demonstrate the importance of this interaction in structural and functional regulation.

Author Contributions

Çağdaş Dağ: Conceptualization, Methodology, Supervision Funding acquisition, Investigation, Formal analysis, Writing- Reviewing and Editing, Writing-Original draft preparation **Alp Eren Kazar:**Investigation, Formal analysis, Visualization, Writing- Reviewing and Editing, Writing-Original draft preparation **Emine Sonay Elgin:** Conceptualization, Methodology, Supervision Funding acquisition, Investigation, Formal analysis, Writing- Reviewing and Editing, Writing-Original draft preparation **Arthur L. Haas:** Conceptualization, Supervision **Kerem Kahraman**: Investigation, Formal analysis, Visualization. **Oktay Göcenler:** Formal analysis, Investigation Writing - Original Draft, Visualization **Mahil Lambert:** Formal analysis, Investigation, Writing - Original Draft, Visualization **Volker Dötsch**: Conceptualization, Supervision, Writing-Reviewing and Editing **Cansu D. Tozkoparan:**Visualization, Formal analysis **Joshua J. Ziarek:** Conceptualization, Writing- Reviewing and Editing

ACKNOWLEDGMENT

We gratefully acknowledge Prof. Brian F. Volkman (Medical College of Wisconsin) for generously opening his laboratory to us and providing access to critical instrumentation and consumables (GM64598-03). His support and willingness to share resources were invaluable for the successful execution of this work. We sincerely thank him for his scientific generosity and hospitality. ESE acknowledges support from TÜBİTAK (Project No: 104T193). CD acknowledges support from TÜBİTAK (Project No: 120Z594, 122Z747). JJZ acknowledges support from National Institutes of Health grant R35GM143054. The authors acknowledge the use of the services and facilities of n^2STAR-Koç University Nanofabrication and Nanocharacterization Center for Scientific and Technological Advanced Research. This study made use of the National Magnetic Resonance Facility at Madison, which is supported by NIH grant R24GM141526 and

P41GM103399. This work benefited from access to [CERM and BMRZ] and has been supported by iNEXT-Discovery, project number 871037, funded by the Horizon 2020 program of the European Commission. Financial support by the Access to Research Infrastructures activity in the 7th Framework Programme of the EC (Project number: 261863, Bio-NMR) for conducting the research is gratefully acknowledged. This study made use of NMRbox: National Center for Biomolecular NMR Data Processing and Analysis, a Biomedical Technology Research Resource (BTRR), which is supported by NIH grant P41GM111135 (NIGMS).

REFERENCES

Afsar, M., Liu, G., Jia, L., Ruben, E. A., Nayak, D., Sayyad, Z., Bury, P. D. S., Cano, K. E., Nayak, A., Zhao, X. R., Shukla, A., Sung, P., Wasmuth, E. V., Gack, M. U., & Olsen, S. K. (2023). Cryo-EM structures of Uba7 reveal the molecular basis for ISG15 activation and E1-E2 thioester transfer. *Nature communications*, *14*(1), 4786. https://doi.org/10.1038/s41467-023-39780-z

Bogunovic, D., Byun, M., Durfee, L. A., Abhyankar, A., Sanal, O., Mansouri, D., Salem, S., Radovanovic, I., Grant, A. V., Adimi, P., Mansouri, N., Okada, S., Bryant, V. L., Kong, X. F., Kreins, A., Velez, M. M., Boisson, B., Khalilzadeh, S., Ozcelik, U., Darazam, I. A., … Casanova, J. L. (2012). Mycobacterial disease and impaired IFN-γ immunity in humans with inherited ISG15 deficiency. *Science (New York, N.Y.)*, *337*(6102), 1684–1688. https://doi.org/10.1126/science.1224026

Bhopatkar AA, Uversky VN, Rangachari V. Disorder and cysteines in proteins: A design for orchestration of conformational see-saw and modulatory functions. Prog Mol Biol Transl Sci. https://10.1016/bs.pmbts.2020.06.001.

Capili, A. D., Lima, C. D. (2007). Structure and analysis of a complex between SUMO and Ubc9 illustrates features of a conserved E2-Ubl interaction. *Journal of molecular biology*, *369*(3), 608–618. https://doi.org/10.1016/j.jmb.2007.04.006

Durfee, L. A., Lyon, N., Seo, K., Huibregtse, J. M. (2010). The ISG15 conjugation system broadly targets newly synthesized proteins: implications for the antiviral function of ISG15. *Molecular cell*, *38*(5), 722–732. https://doi.org/10.1016/j.molcel.2010.05.002

de Vries, S. J., van Dijk, M., Bonvin, A. M. (2010). The HADDOCK web server for data-driven biomolecular docking. *Nature protocols*, *5*(5), 883–897. https://doi.org/10.1038/nprot.2010.32

Elgin, E. S., Sökmen, N., Peterson, F. C., Volkman, B. F., Dağ, C., Haas, A. L. (2012). E2-binding surface on Uba3 β-grasp domain undergoes a conformational transition. *Proteins*, *80*(10), 2482–2487. https://doi.org/10.1002/prot.24148

Farrell, P. J., Broeze, R. J., Lengyel, P. (1979). Accumulation of an mRNA and protein in interferon-treated Ehrlich ascites tumour cells. *Nature*, *279*(5713), 523–525. https://doi.org/10.1038/279523a0.

Haas, A.L. (2007). ISG15-dependent Regulation. In Protein Degradation Series (eds R.J. Mayer, A.J. Ciechanover and M. Rechsteiner). https://doi.org/10.1002/9783527619320.ch5b

Huang, D. T., Paydar, A., Zhuang, M., Waddell, M. B., Holton, J. M., & Schulman, B. A. (2005). Structural basis for recruitment of Ubc12 by an E2 binding domain in NEDD8's E1. Molecular cell, 17(3), 341-350

Jubb, H., Blundell, T. L., Ascher, D. B. (2015). Flexibility and small pockets at protein-protein interfaces: New insights into druggability. *Progress in biophysics and molecular biology*, *119*(1), 2–9. https://doi.org/10.1016/j.pbiomolbio.2015.01.009

Lakomek, N. A., Ying, J., Bax, A. (2012). Measurement of ^{15}N relaxation rates in perdeuterated proteins by TROSY-based methods. *Journal of biomolecular NMR*, *53*(3), 209–221. https://doi.org/10.1007/s10858-012-9626-5

Lee, W., Rahimi, M., Lee, Y., Chiu, A. (2021). POKY: a software suite for multidimensional NMR and 3D structure calculation of biomolecules, *Bioinformatics*, Volume 37, Issue 18, Pages 3041–3042, https://doi.org/10.1093/bioinformatics/btab180

Loeb, K. R., Haas, A. L. (1992). The interferon-inducible 15-kDa ubiquitin homolog conjugates to intracellular proteins. *The Journal of biological chemistry*, *267*(11), 7806–7813.

Lois, L. M., & Lima, C. D. (2005). Structures of the SUMO E1 provide mechanistic insights into SUMO activation and E2 recruitment to E1. *The EMBO journal*, *24*(3), 439-451.

Lv, Z., Williams, K.M., Yuan, L., Atkison, JH, Olsen SK. Crystal structure of a human ubiquitin E1-ubiquitin complex reveals conserved functional elements essential for activity. J Biol Chem. 2018 Nov 23;293(47):18337-18352. doi: 10.1074/jbc.RA118.003975

Mazmanian, K., Sargsyan, K., Grauffel, C., Dudev, T., & Lim, C. (2016). Preferred Hydrogen-Bonding Partners of Cysteine: Implications for Regulating Cys Functions. *The journal of physical chemistry. B*, *120*(39), 10288–10296. https://doi.org/10.1021/acs.jpcb.6b08109

Narasimhan, J., Potter, J. L., Haas, A. L. (1996). *Conjugation of the 15-kDa Interferon-induced Ubiquitin Homolog Is Distinct from That of Ubiquitin. Journal of Biological Chemistry, 271(1), 324–330.* doi:10.1074/jbc.271.1.324

Olsen, S. K., & Lima, C. D. (2013). Structure of a ubiquitin E1-E2 complex: insights to E1-E2 thioester transfer. Molecular cell, 49(5), 884-896.

Poller, W., Knobeloch, K. P., Voigt, A. (2014). Ubiquitin-like protein ISG15 (interferon-stimulated gene of 15 kDa) in host defense against heart failure in a mouse model of virus-induced cardiomyopathy. *Circulation*, *130*(18), 1589–1600. https://doi.org/10.1161/CIRCULATIONAHA.114.009847

Rahnefeld, A., Klingel, K., Schuermann, A., Diny, N. L., Althof, N., Lindner, A., … Voigt, A. (2014). *Ubiquitin-Like Protein ISG15 (Interferon-Stimulated Gene of 15 kDa) in Host Defense Against Heart Failure in a Mouse Model of Virus-Induced CardiomyopathyCLINICAL PERSPECTIVE. Circulation, 130(18), 1589–1600.* doi:10.1161/circulationaha.114

Sadler, A. J., Williams, B. R. (2008). Interferon-inducible antiviral effectors. *Nature reviews. Immunology*, *8*(7), 559–568. https://doi.org/10.1038/nri2314

Shen, Y., Delaglio, F., Cornilescu, G. et al. TALOS+: a hybrid method for predicting protein backbone torsion angles from NMR chemical shifts. J Biomol NMR 44, 213–223 (2009).

Streich, F.C., Haas, A.L. (2010). Activation of Ubiquitin and Ubiquitin-Like Proteins. In: Groettrup, M. (eds) Conjugation and Deconjugation of Ubiquitin Family Modifiers. Subcellular Biochemistry, vol 54. Springer, New York, NY. https://doi.org/10.1007/978-1-4419-6676-6_1

Wang, J., Taherbhoy, A. M., Hunt, H. W., Seyedin, S. N., Miller, D. W., Miller, D. J., Huang, D. T., & Schulman, B. A. (2010). Crystal structure of UBA2(ufd)-Ubc9: insights into E1-E2 interactions in Sumo pathways. *PloS one*, *5*(12), e15805. https://doi.org/10.1371/journal.pone.0015805

Zhang, M., Li, J., Yan, H., Huang, J., Wang, F., Liu, T., Zeng, L., Zhou, F. (2021). ISGylation in Innate Antiviral Immunity and Pathogen Defense Responses: A Review. *Frontiers in cell and developmental biology*, *9*, 788410. https://doi.org/10.3389/fcell.2021.788410

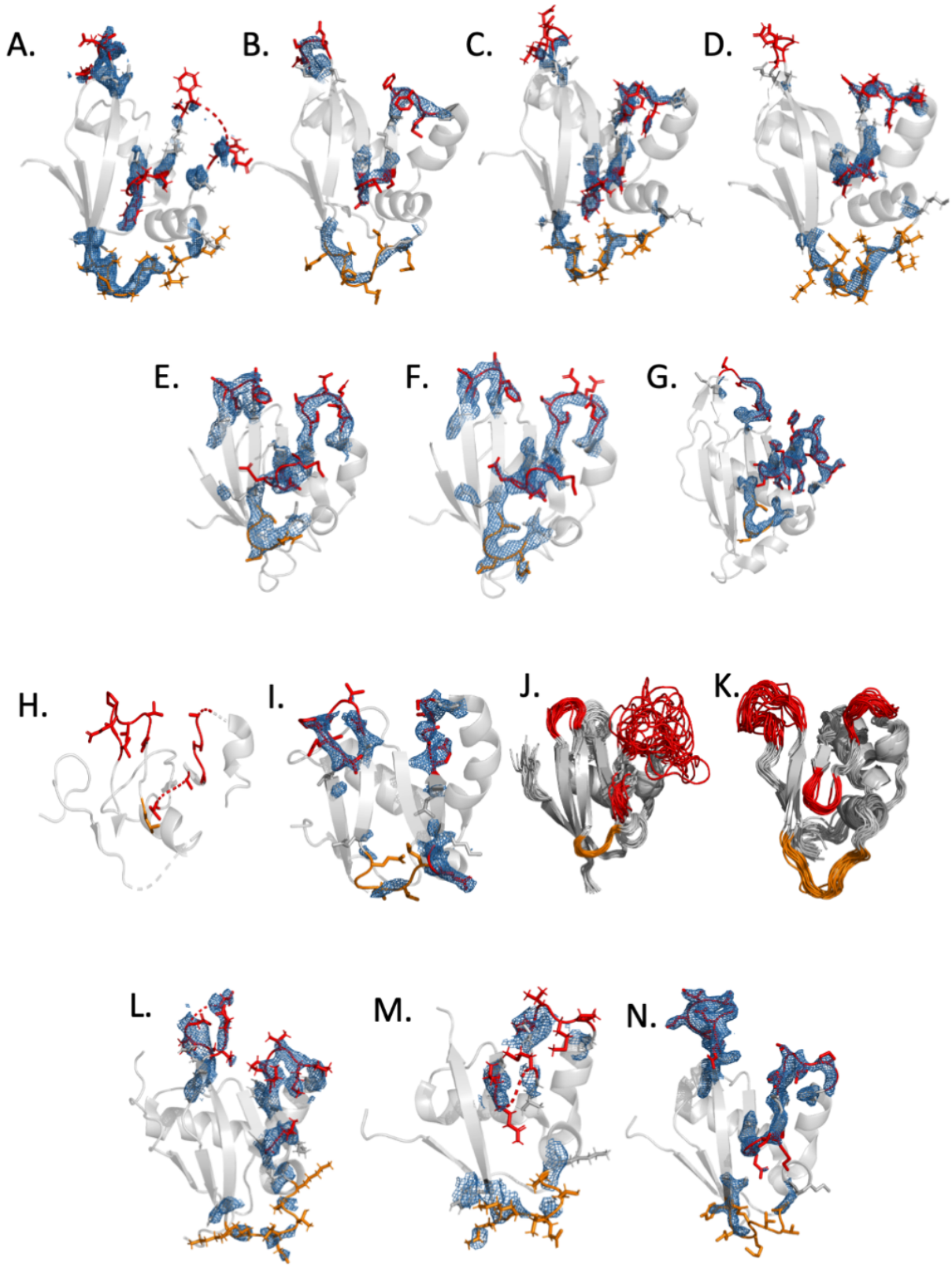

691

692 Figure 1. Ubiquitin and Ubiquitin-like post-translational modification systems E1 enzymes' ubiquitin fold
693 domain structures. Regions on the structures that have high plasticity and directly interact with E2 are
694 marked in red, and regions thought to interact with Ubl are marked in orange. Electron density maps are
695 also shown over the colored regions. A. Saccharomyces cerevisiae Uba1 Apo form (PDB: 7ZH9) B. Homo
696 sapiens Uba1 complex with ubiquitin (PDB: 6DC6) C. Saccharomyces cerevisiae complex with Ubc13
697 (E2) (PDB: 6ZHS) D. Schizosaccharomyces pombe complex with Ubc15 (E2) and ubiquitin (PDB: 5KNL)
698 E. Homo sapiens Uba2 apo form (6CWZ) F. Homo sapiens Uba2 complex with SUMO (3KYC) G.
699 Saccharomyces cerevisiae Uba2-UFD complex with Ubc9 (3ONG) H. Homo sapiens Uba3 apo form
700 (1YOV) I. Homo sapiens Uba3-UFD complex with Ubc12 (1Y8X) J. Homo sapiens Uba3 UFD apo form
701 (2LQ7) K. Homo sapiens Uba7-UFD apo form (8WWX) L. Homo sapiens apo Uba6 (7PVN) M. Homo
702 sapiens Uba6 complex with FAT10 (7PYV) N. Homo sapiens Uba6 complex with FAT10 (7SOL)
703
704

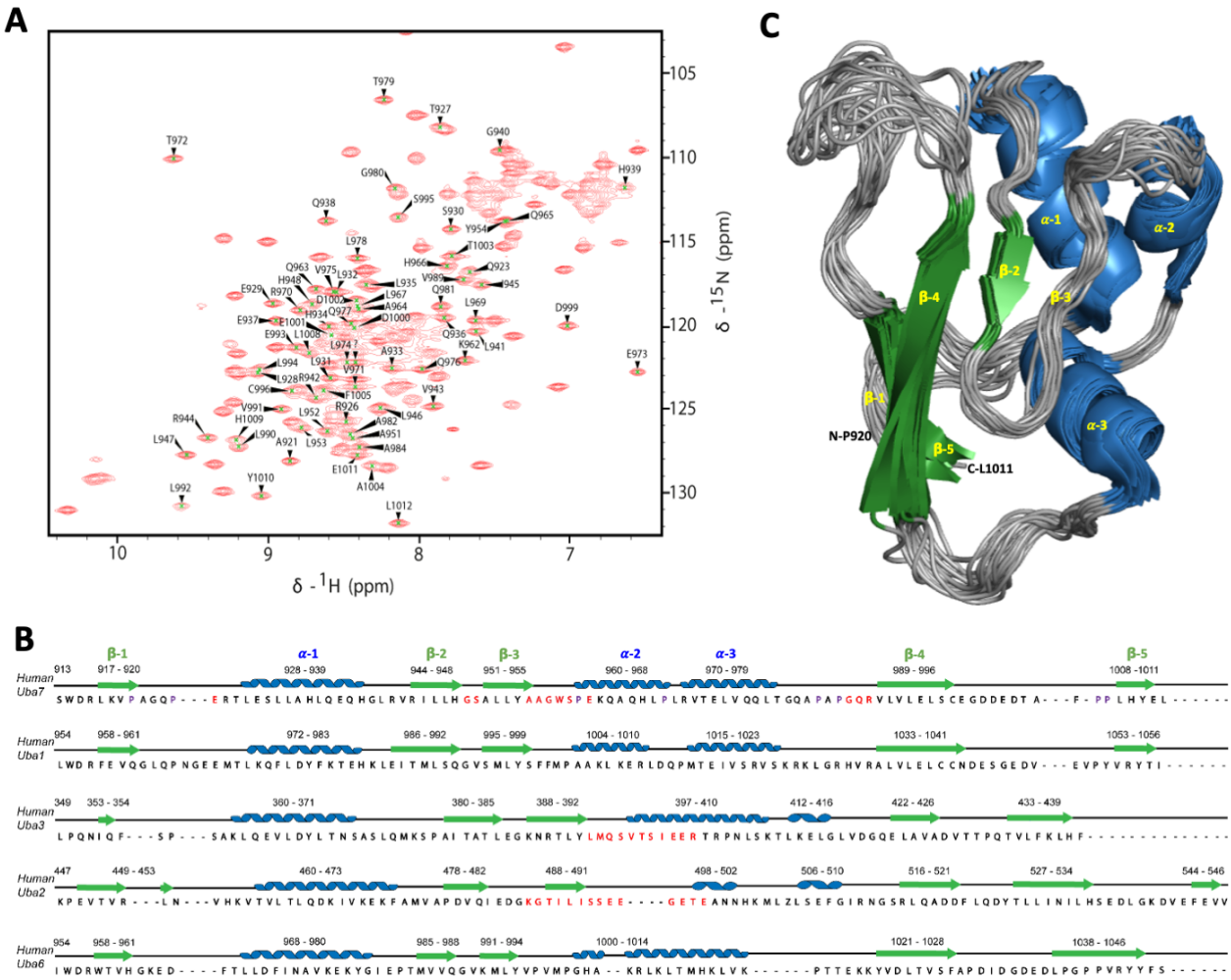

Figure 2. NMR structure of Human Uba7 ubiquitin fold domain A. Human Uba7 enzyme ubiquitin fold domain ^{1}H-^{15}N HSQC spectrum and N-H assignments. B. Human Ubiquitin-like systems activating enzymes ubiquitin fold domain sequential and secondary structure alignment C. Superposition of the 20 lowest-energy NMR structures of the Uba7 ubiquitin fold domain

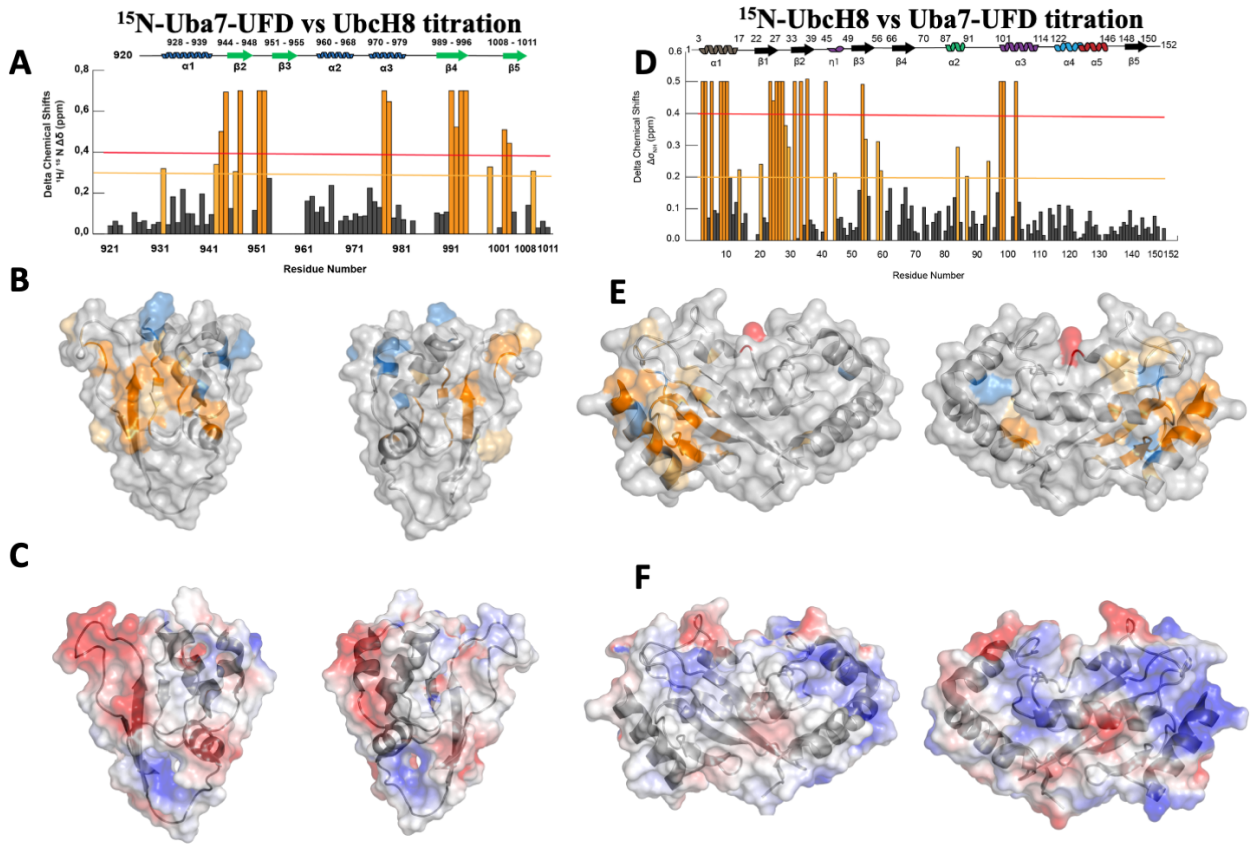

Figure 3. Mapping of interactions between UbcH8 and Uba7-UFD at the amino acid level and NMR data driven modeling of the Uba7-UbcH8 complex structure A. ^{15}N-Uba7-UFD vs UbcH8 titration Chemical Shift Perturbation graph ^{1}H-^{15}N chemical shift perturbations for Uba7-UFD were calculated for each residue. The residues colored orange possessed chemical shift perturbations larger than 0.4 ppm threshold (red line). The residue colored merigold possessed chemical shift perturbations larger than the 0.3 ppm threshold (merigold line). B. ^{15}N-Uba7-UFD vs UbcH8 titration Chemical Shift Perturbation map Residues with chemical shift perturbations larger than the 0.4 ppm threshold (red), residues with chemical shift perturbations larger than 0.3 ppm threshold (merigold) and peak intensity changes that were larger than the threshold (blue) were mapped onto the Uba7-UFD structure C. Surface electrostatic potential of Uba7-UFD Red and blue coloured regions denote negative and positive charges, respectively. D. ^{15}N-UbcH8 vs Uba7-UFD Titration Chemical Shift Perturbation graph ^{1}H-^{15}N chemical shift perturbations for UbcH8 were calculated for each residue. The residues colored orange possessed chemical shift perturbations larger than

728 0.4 ppm threshold (red line). The residues colored merigold possessed chemical shift perturbations larger
729 than the 0.2 ppm threshold (merigold line). E. ^{15}N-UbcH8 vs Uba7-UFD Titration Chemical Shift
730 Perturbation map Residues with chemical shift perturbations larger than the 0.4 ppm threshold (orange),
731 residues with chemical shift perturbations larger than 0.2 ppm threshold (merigold) and peak intensity
732 changes that were larger than the threshold (blue) were mapped onto the UbcH8 crystal structure (PDB
733 1WZV), red residue represents the active-site cysteine (Cys85) of UbcH8 involved in transthiolation. F.
734 Surface electrostatic potential of UbcH8 Red and blue coloured regions denote negative and positive
735 charges, respectively.
736
737
738
739
740
741
742
743
744
745
746
747
748
749

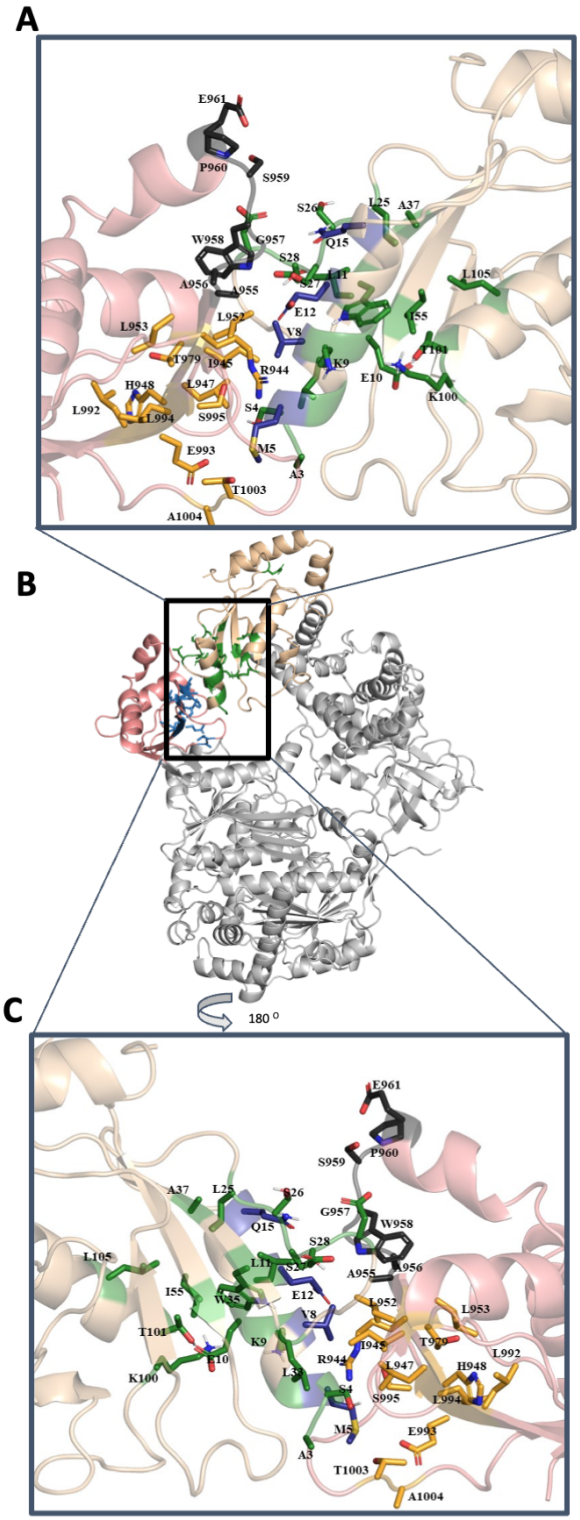

750

751 Figure 4. NMR data driven model of the Uba7-UbcH8 complex structure

752

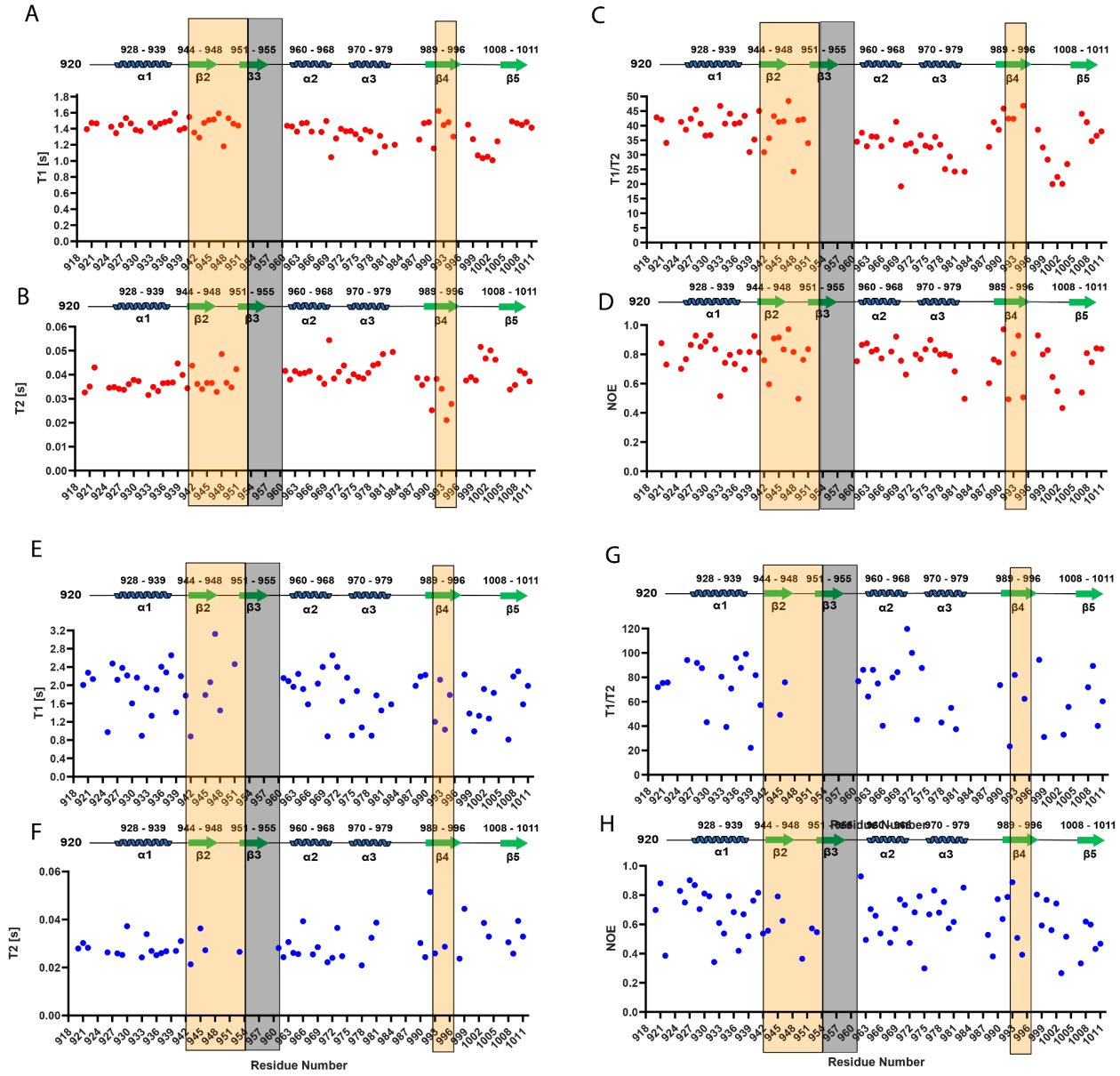

Figure 5. ^{15}N Relaxation analysis for Uba7 UFD and Uba7 UFD-UbcH8 complex A. ^{15}N T1 relaxation rate as function of Uba7 UFD sequence B. ^{15}N T2 relaxation rate as function of Uba7 UFD sequence C. T1/T2 values of Uba7 UFD protein as function of Uba7 UFD sequence D. ^{1}H-^{15}N NOE relaxation analysis for Uba7 UFD E. ^{15}N T1 relaxation rates of ^{15}N-labeled Uba7 in complex with unlabeled UbcH8 F. ^{15}N T2 relaxation rates of ^{15}N-labeled Uba7 in complex with unlabeled UbcH8 G. T1/T2 relaxation values of ^{15}N-labeled Uba7 UFD in complex with unlabeled UbcH8, plotted as a function of the Uba7 UFD sequence H. ^{1}H-^{15}N NOE relaxation analysis for Uba7 UFD in complex with unlabeled UbcH8

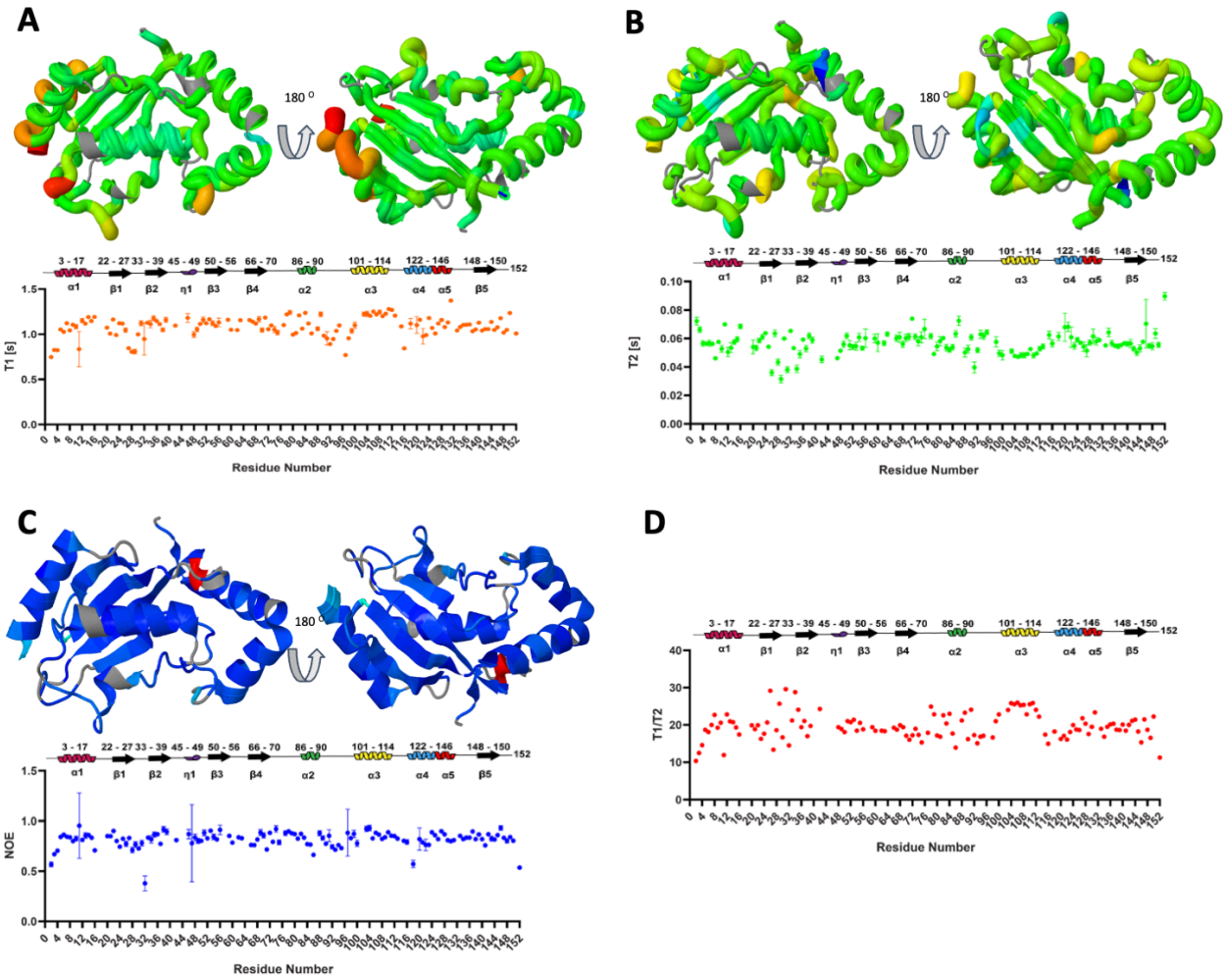

Figure 6. ^{15}N Relaxation analysis for UbcH8 A. ^{15}N T1 relaxation rate as function of protein sequence and mapped on crystal structure (PDB:1WZW) B. ^{15}N T2 relaxation rate as function of protein sequence and mapped on crystal structure (PDB:1WZW) C. ^{1}H-^{15}N NOE relaxation analysis for UbcH8 and mapped on crystal structure (PDB:1WZW) D. T1/T2 values of UbcH8 protein as function of protein sequence

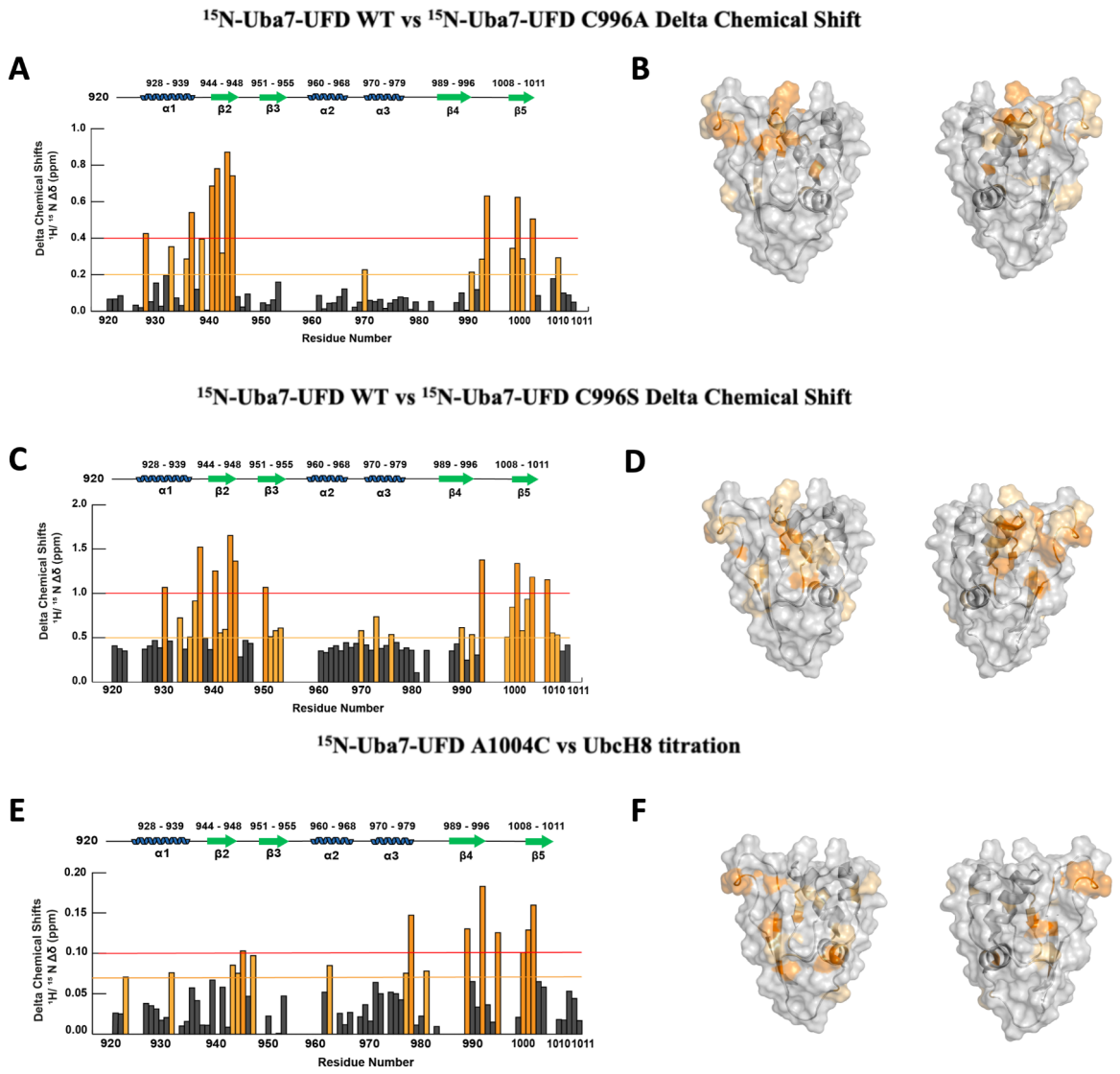

Figure 7. Investigation of the Effects of Mutations on ^{1}H-^{15}N Chemical Shift Values of Uba7-UFD A. ^{15}N-Uba7-UFD WT vs ^{15}N-Uba7-UFD C996A Delta Chemical Shift Map The residues colored orange possessed delta chemical shift larger than 0.4 ppm threshold (red line). The residues colored merigold possessed delta chemical shift larger than the 0.2 ppm threshold (merigold line). B.^{15}N-Uba7-UFD WT vs ^{15}N-Uba7-UFD C996A significant Delta Chemical Shifts Mapped on protein structure Residues with delta chemical shift larger than 0.4 ppm threshold (orange), residues with chemical shift perturbations larger than 0.2 ppm threshold (merigold) were mapped onto the Uba7-UFD structure C. ^{15}N-Uba7-UFD WT vs ^{15}N-Uba7-UFD C996S Delta Chemical Shift Map The residues colored orange possessed delta chemical shift

775 larger than 1 ppm threshold (red line). The residues colored merigold possessed delta chemical shift larger
776 than the 0.5 ppm threshold (merigold line). D. ^{15}N-Uba7-UFD WT vs ^{15}N-Uba7-UFD C996S significant
777 Delta Chemical Shifts Mapped on protein structure Residues with delta chemical shift larger than 1 ppm
778 threshold (orange), residues with chemical shift perturbations larger than 0.5 ppm threshold (merigold)
779 were mapped onto the Uba7-UFD structure E. ^{15}N-Uba7-UFD A1004C vs UbcH8 titration Chemical Shift
780 Perturbation Map ^{1}H-^{15}N chemical shift perturbations for Uba7-UFD were calculated for each residue. The
781 residues colored orange possessed chemical shift perturbations larger than 0.1 ppm threshold (red line). The
782 residues colored merigold possessed chemical shift perturbations larger than the 0.06 ppm threshold
783 (merigold line). F. ^{15}N-Uba7-UFD A1004C significant Chemical Shift Perturbations Mapped on protein
784 structure Residues with chemical shift perturbations larger than the 0.1 ppm threshold (orange), residues
785 with chemical shift perturbations larger than 0.06 ppm threshold (merigold) and peak intensity changes that
786 were larger than the threshold (blue) were mapped onto the Uba7-UFD structure
787
788
789
790
791
792
793
794
795
796

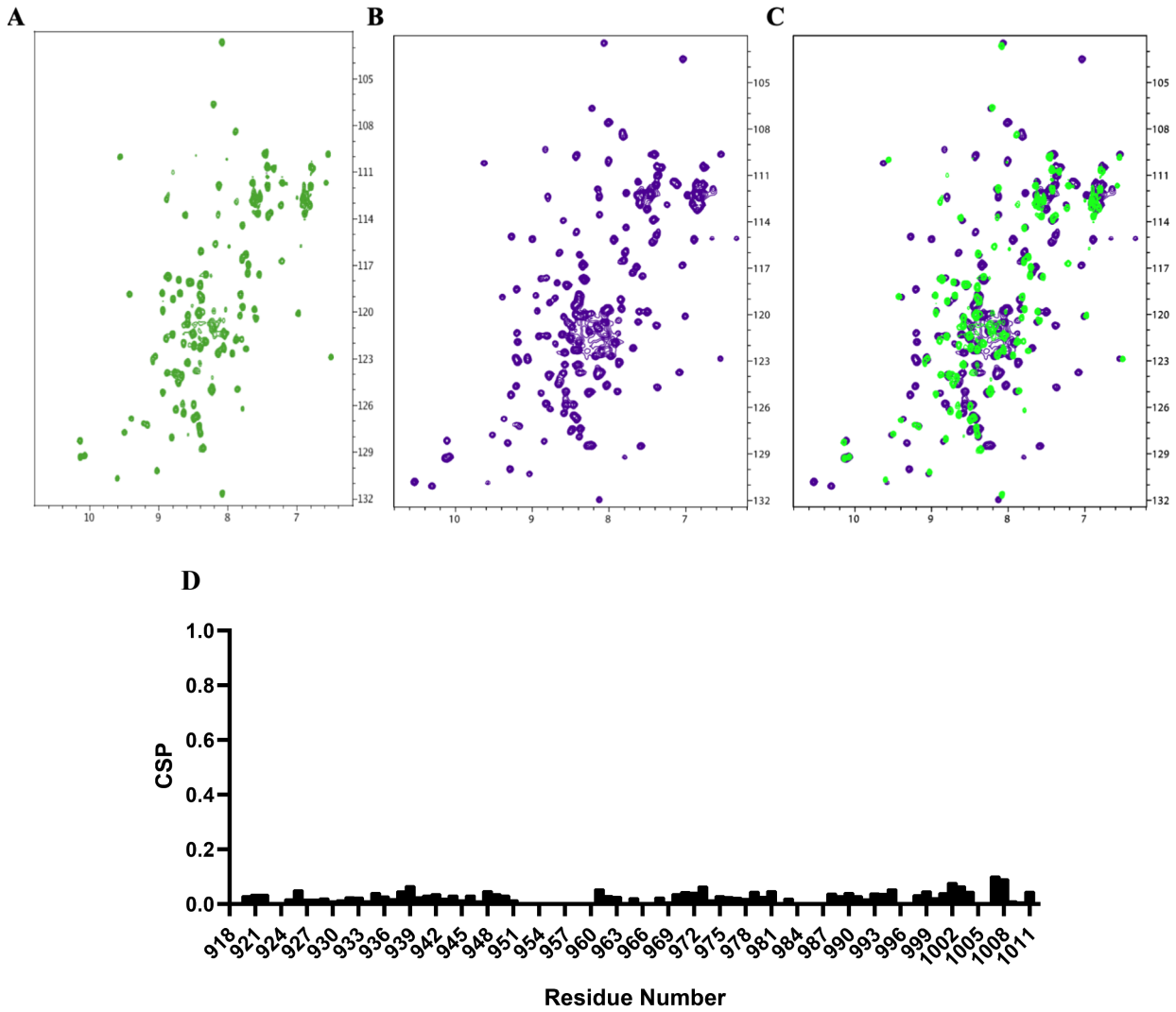

Supplementary Figure 1. Human Uba7 enzyme ubiquitin fold domain ^{1}H-^{15}N HSQC spectrum A. ^{1}H-^{15}N HSQC spectrum of Uba7-UFD after GBI fusion protein cut. B. ^{1}H-^{15}N HSQC spectrum of GBI-Uba7-UFD C. ^{1}H-^{15}N HSQC spectrum of GBI-Uba7-UFD overlaid with ^{1}H-^{15}N HSQC spectrum of Uba7-UFD after GBI fusion protein cut D. Chemical shift perturbations (CSPs) analysis of Uba7-UFD with and without the GB1 fusion tag.

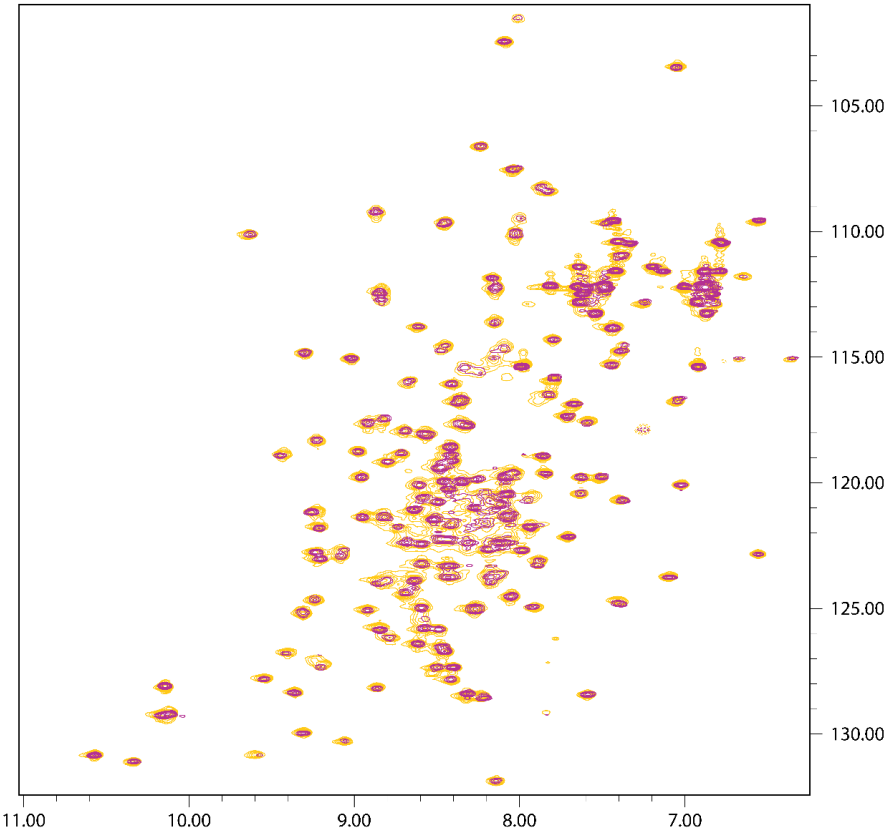

Supplementary Figure 2. ^{1}H-^{15}N HSQC spectrum of 0.4 mM ^{15}N-GBI-Uba7-UFD (wt) protein (yellow on day 1, red on day 9)

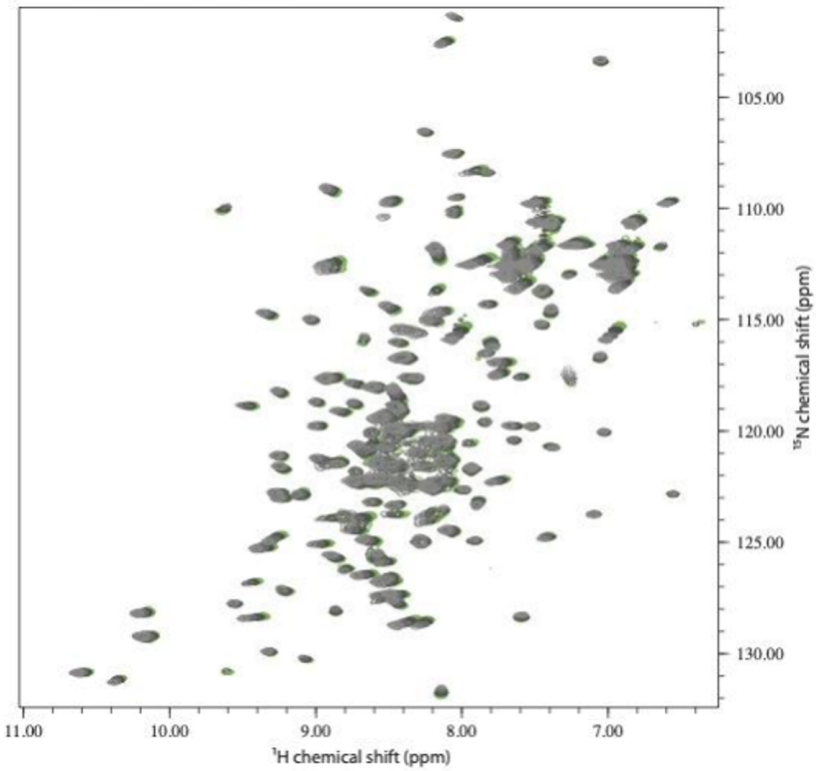

Supplementary Figure 3. Overlay of ^{15}N-GBI-Uba7-UFD ^{1}H-^{15}N HSQC spectra at different temperatures. (green 25°C, black 20°C, dark gray 15°C, light gray 10°C)

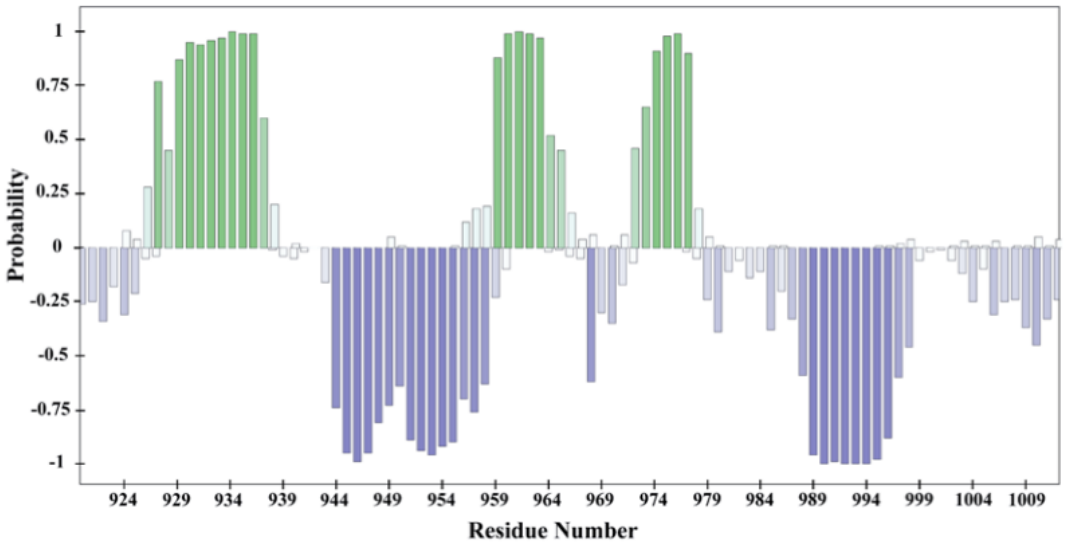

822

823 Supplementary Figure 4. NMR chemical-shift-based TALOS-N secondary-structure prediction of Uba7-

824 UFD

825

826

827

828

829

830

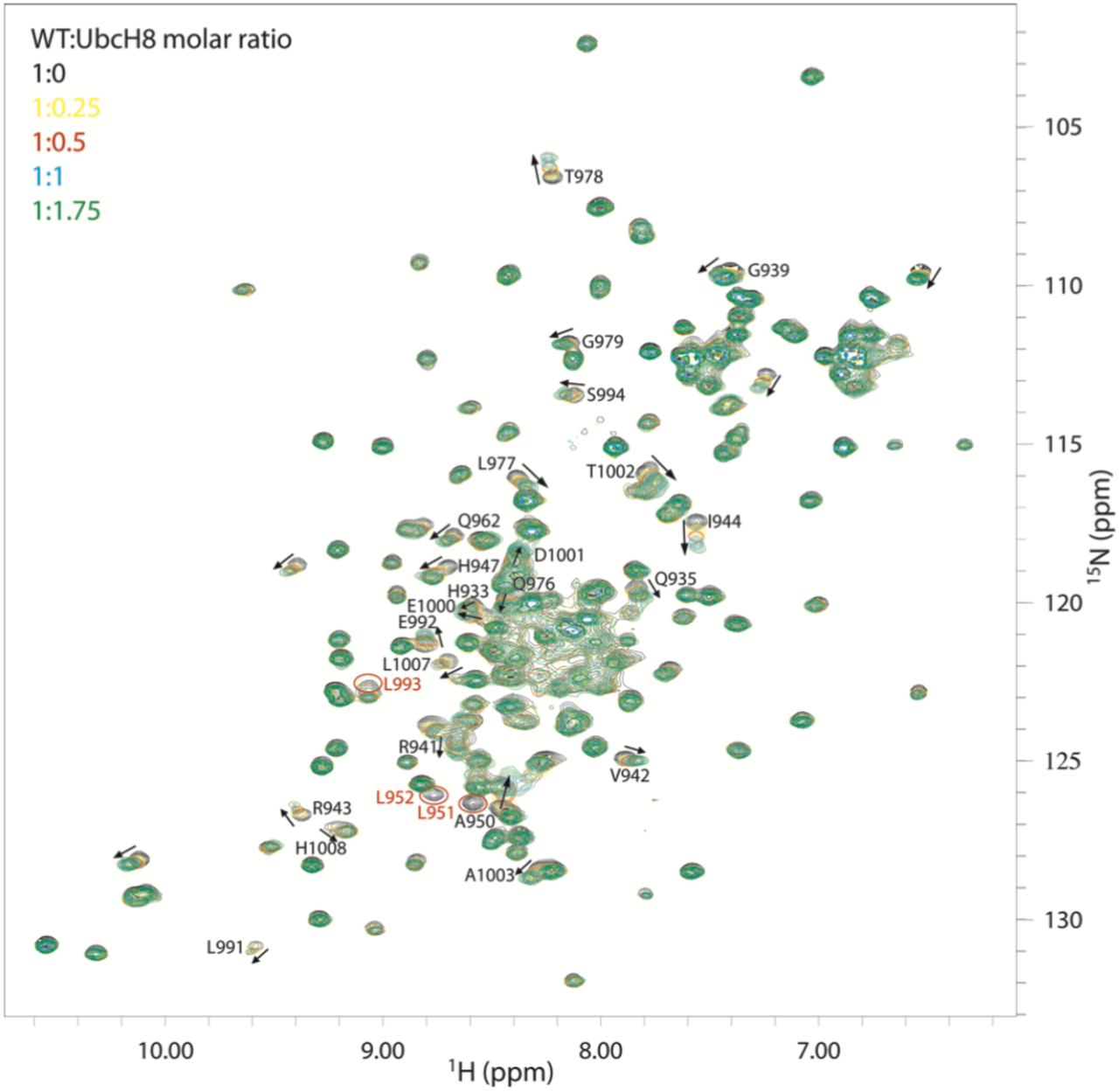

Supplementary Figure 5. Superposition of the ^{1}H-^{15}N HSQC spectra of free (black) and various amounts of UbcH8 bound forms of wild type ^{15}N-GBI-Uba7-UFD. GBI-Uba7-UFD:UbcH8 molar ratios in the bound forms are indicated in yellow for 1:0.25, red for 1:0.5, blue for 1:1, and green for 1:1.75. Peaks that disappear upon addition of 1:0.25 molar ratio of UbcH8 are indicated with red circles. Residues that show combined chemical shift perturbations of larger than 0.2 are indicated with an arrow and black one letter code followed by the residue number.

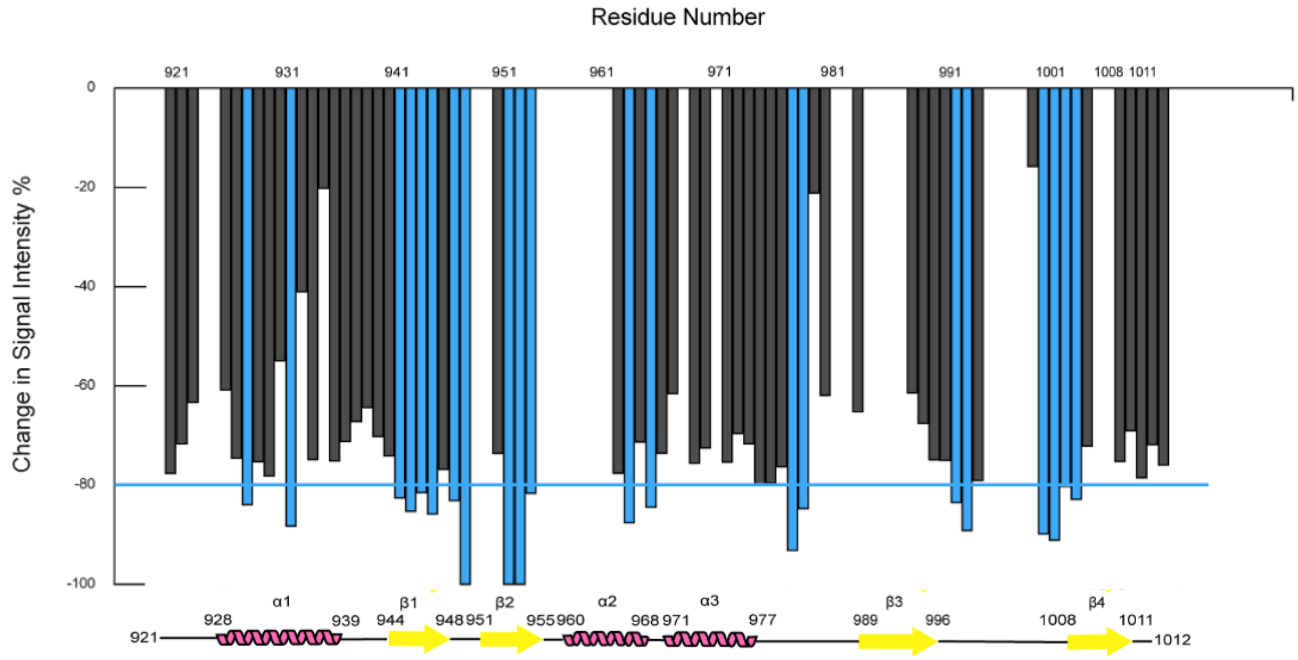

Supplementary Figure 6. ^{15}N-Uba7-UFD vs UbcH8 titration Delta Chemical Shift Intensity Graph ^{1}H-^{15}N HSQC peak intensity changes for Uba7-UFD were calculated for each residue. The residues colored blue possessed peak intensity changes that were larger than the threshold (blue line)

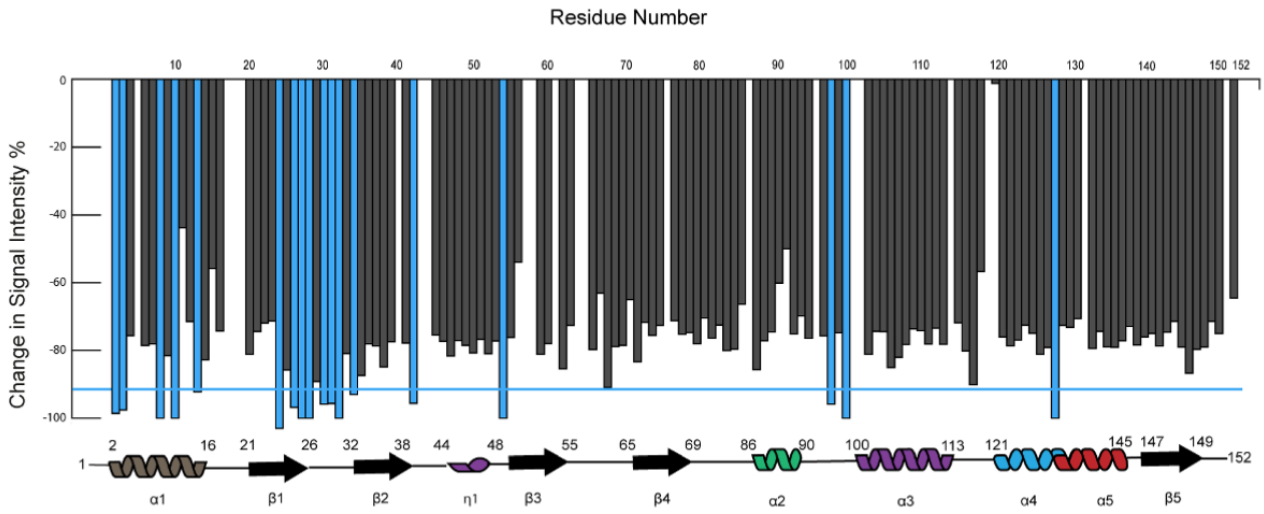

853

854 Supplementary Figure 7. ^{15}N-UbcH8 vs Uba7-UFD titration Delta Chemical Shift Intensity Graph ^{1}H-^{15}N

855 HSQC peak intensity changes for UbcH8 were calculated for each residue. The residues colored blue

856 possessed peak intensity changes that were larger than the threshold (blue line)

857

858

859

860

861

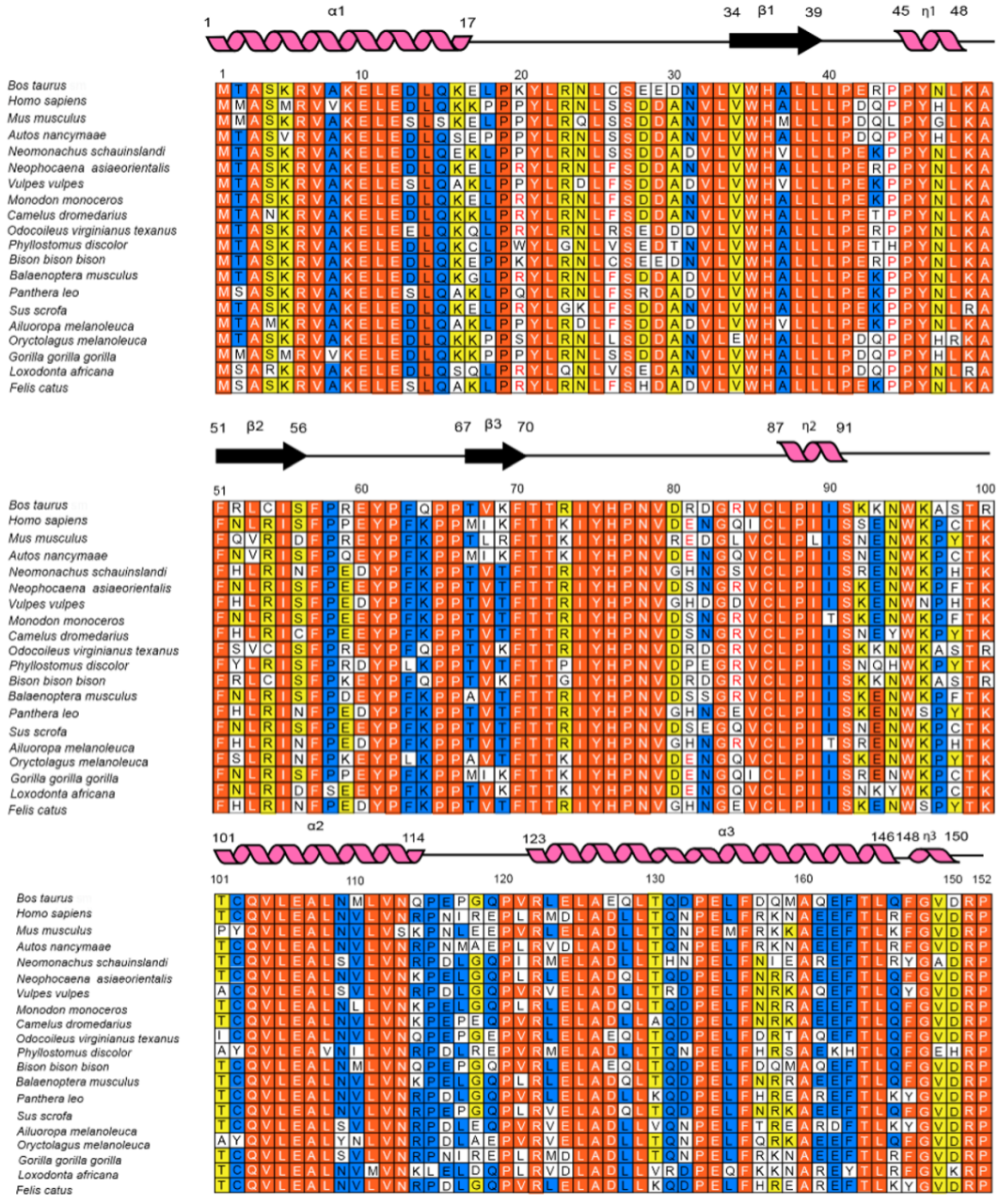

Supplementary Figure 8. Sequence alignment of UbcH8 from different organisms.

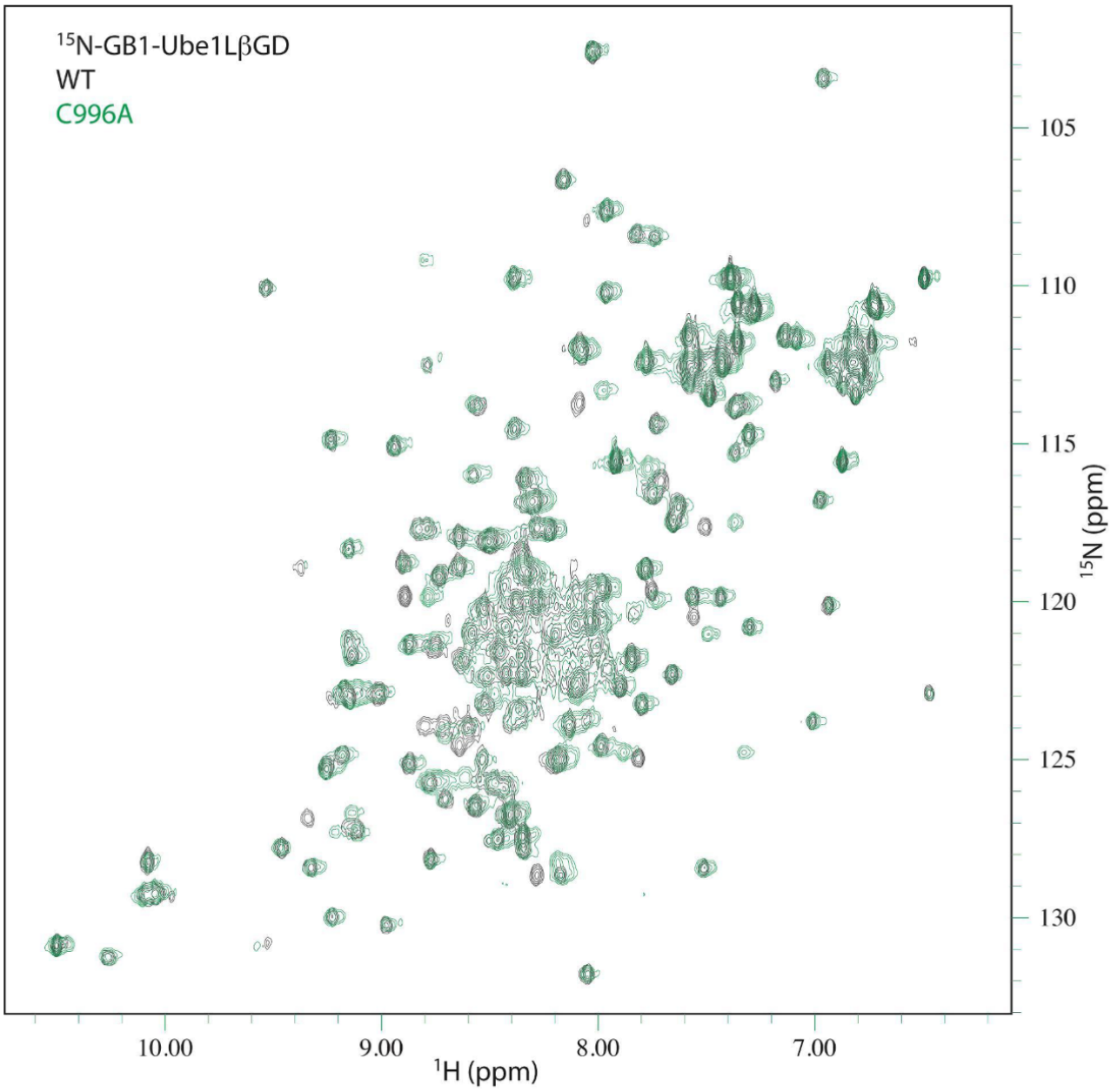

867

868 Supplementary Figure 9. Superposition of 2D ^{1}H-^{15}N HSQCs of wt ^{15}N-GBI-Uba7-UFD (black) with,

869 C996A mutant (green).

870

871

872

873

874

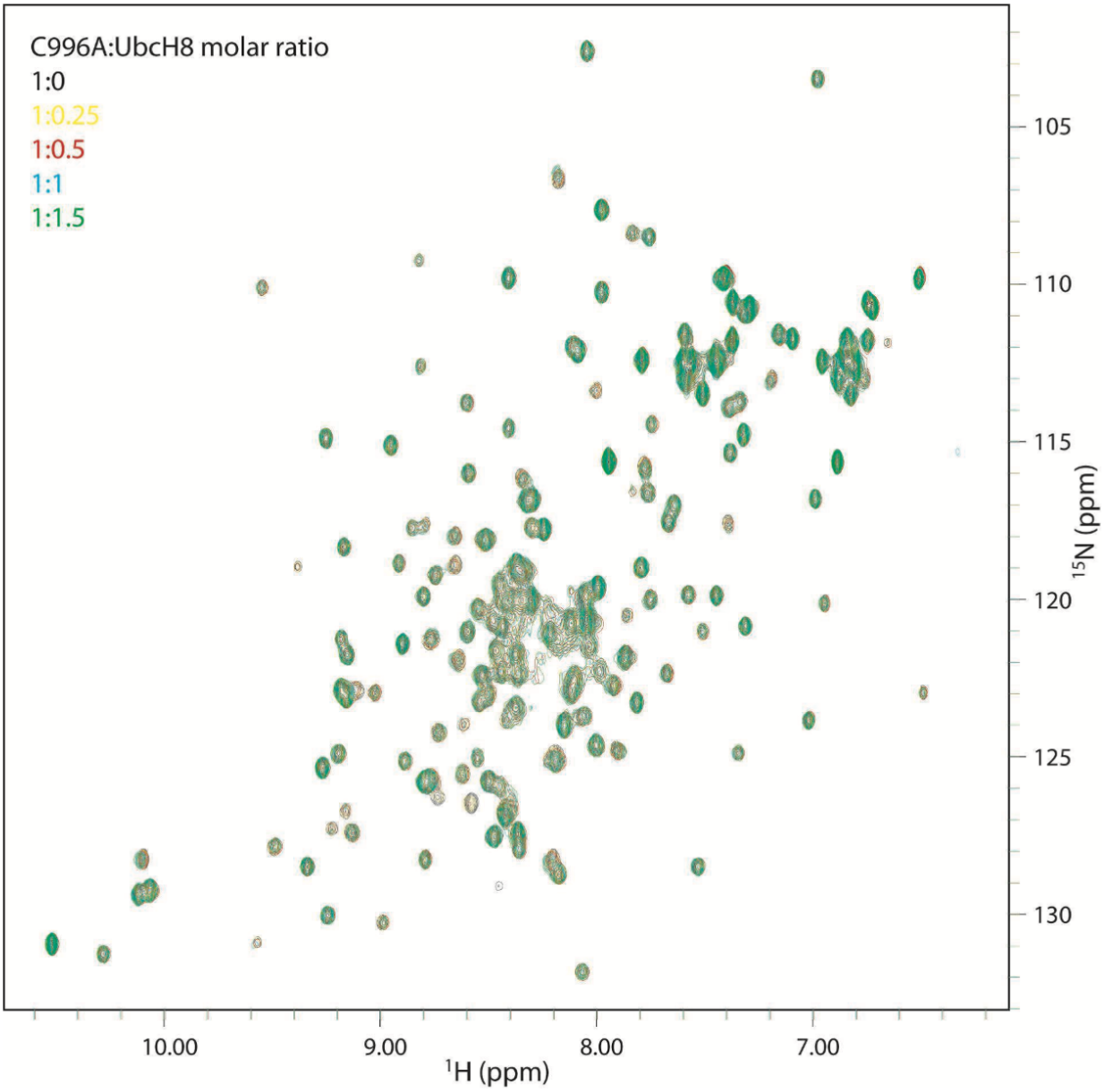

875

876 Supplementary Figure 10. Superposition of the ^{1}H-^{15}N HSQC spectra of free (black) and various amounts

877 of UbcH8 bound forms of ^{15}N-GBI-Uba7-UFD, C996A mutant. GBI-Uba7-UFD:UbcH8 molar ratios in

878 the bound forms are indicated in yellow for 1:0.25, red for 1:0.5, blue for 1:1, and green for 1:1.5.

879

880

881

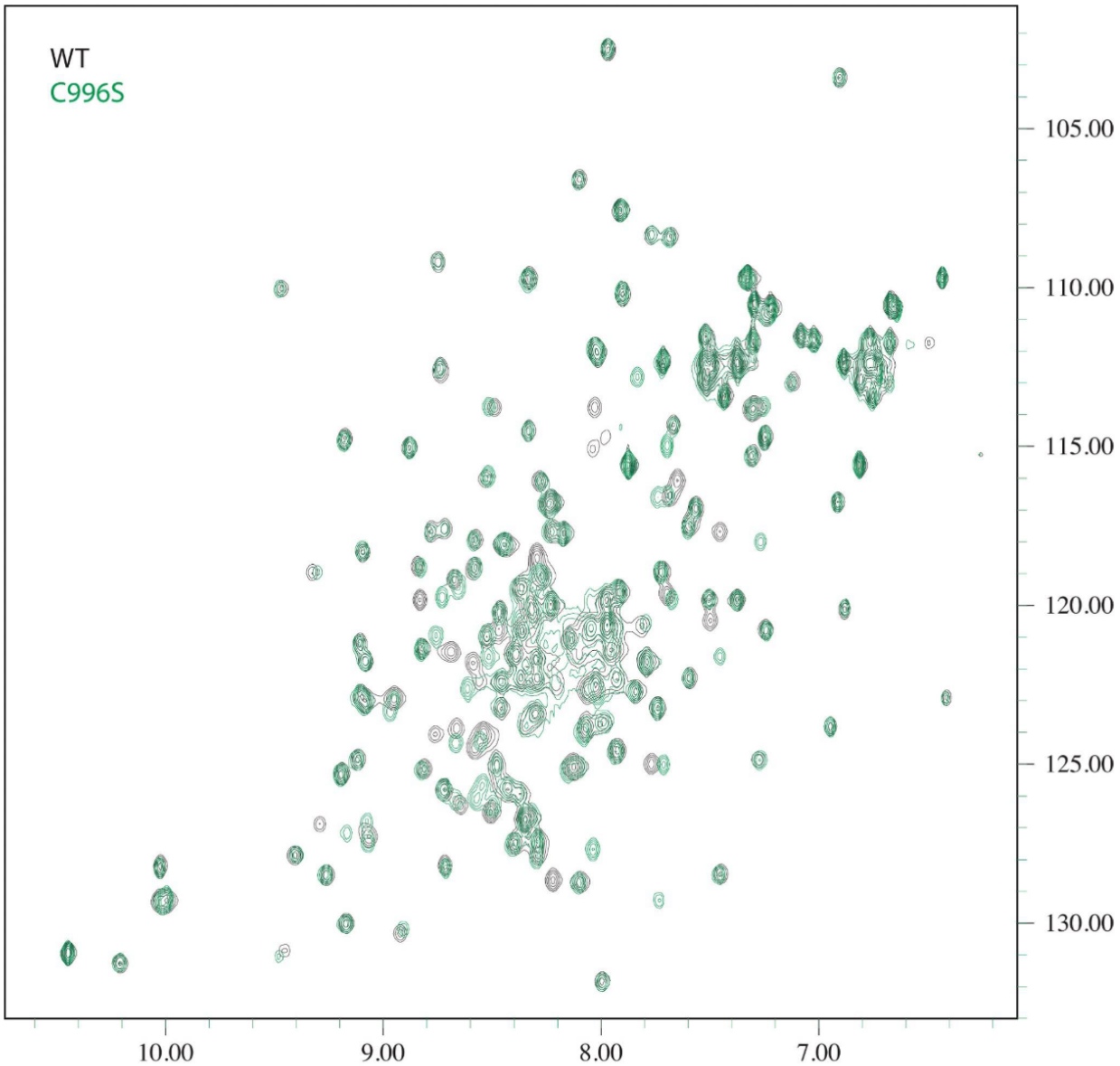

Supplementary Figure 11. Superposition of 2D ^{1}H-^{15}N HSQCs of wt ^{15}N-GBI-Uba7-UFD (black) with, C996S mutant (green).

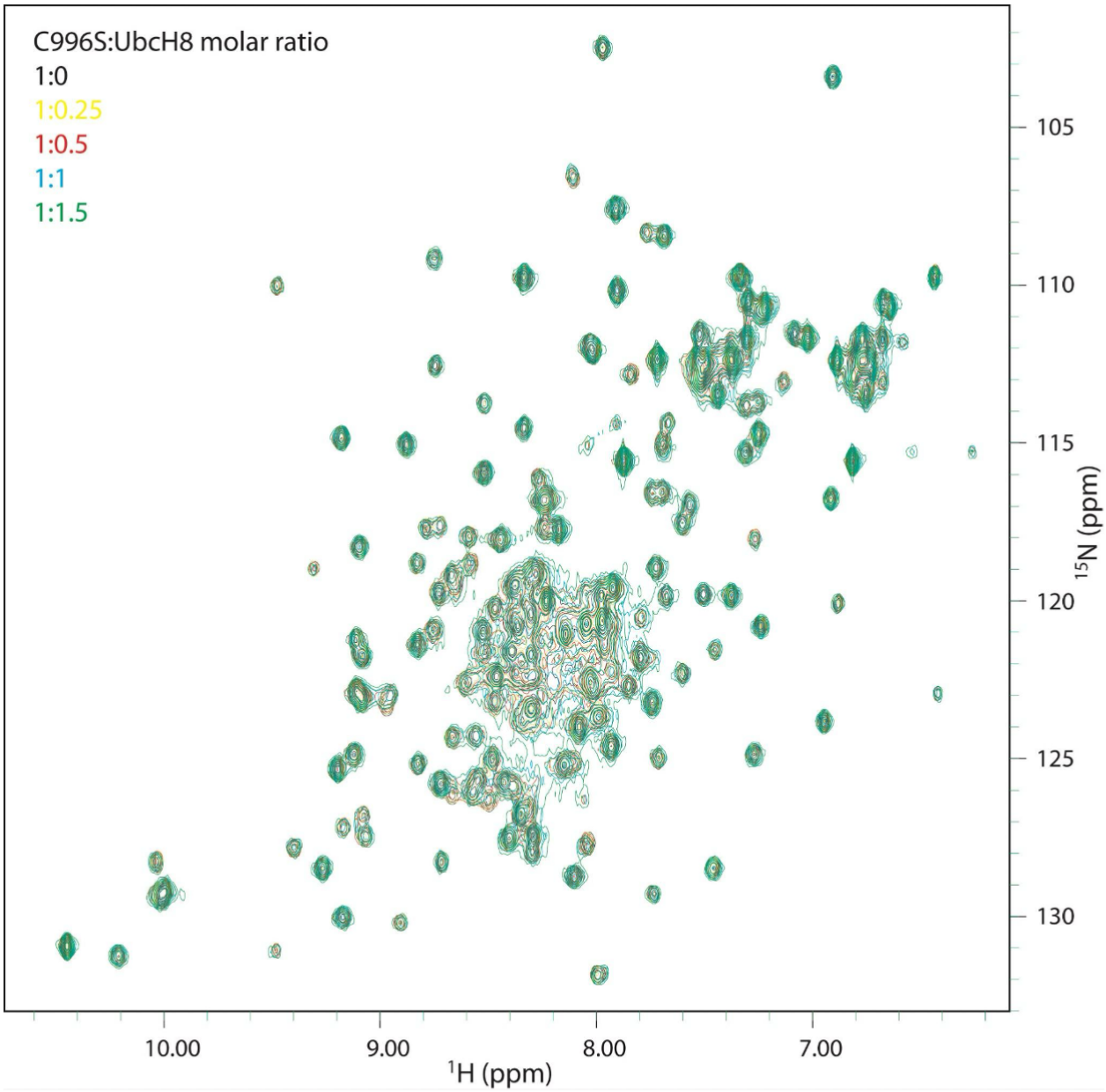

890

891 Supplementary Figure 12. Superposition of the ^{1}H-^{15}N HSQC spectra of free (black) and various amounts

892 of UbcH8 bound forms of ^{15}N-GBI-Uba7-UFD, C996S mutant. GBI-Uba7-UFD:UbcH8 molar ratios in the

893 bound forms are indicated in yellow for 1:0.25, red for 1:0.5, blue for 1:1, and green for 1:1.5.

894

895

896

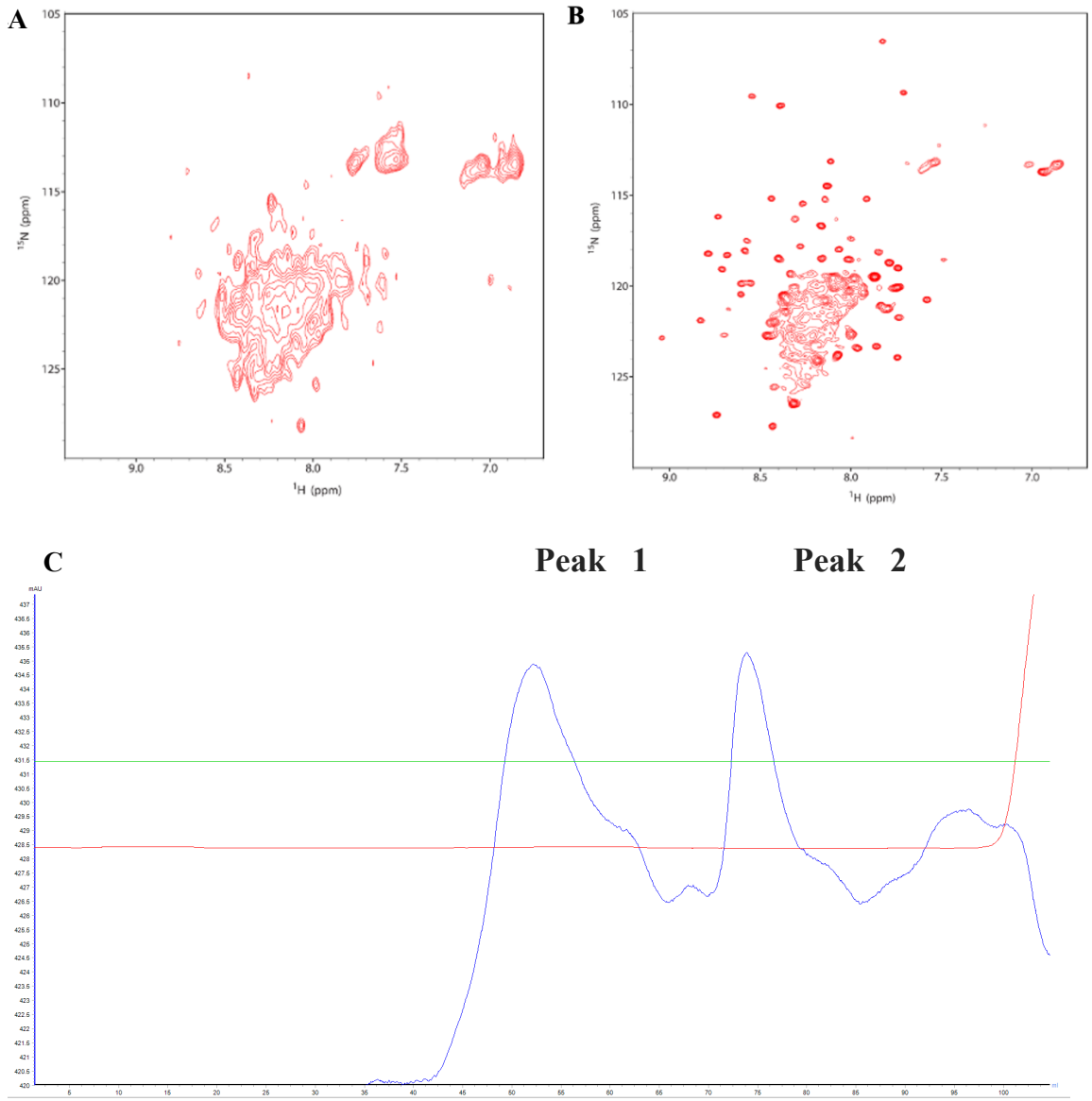

Supplementary Figure 13. ^{1}H-^{15}N HSQC spectra of free form of R944L mutant ^{15}N-GBI-Uba7-UFD. A. ^{1}H-^{15}N HSQC spectrum from first gel filtration peak. B. ^{1}H-^{15}N HSQC spectrum from second gel filtration peak. C. S75 GF chromatogram

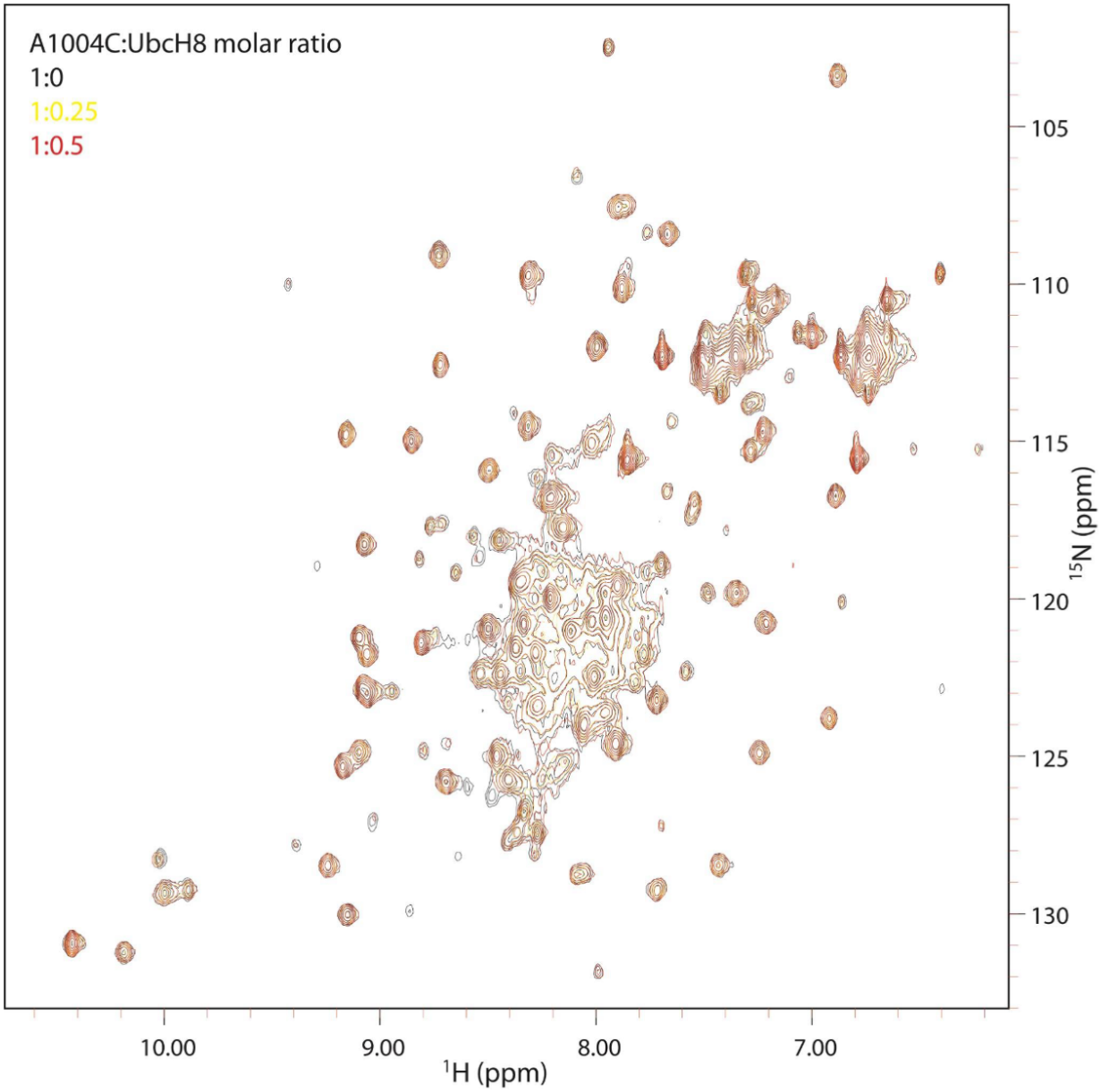

Supplementary Figure 14. Superposition of the ^{1}H-^{15}N HSQC spectra of free (black) and various amounts of UbcH8 bound forms of ^{15}N-GBI-Uba7-UFD, A1004C mutant. GBI-Uba7-UFD:UbcH8 molar ratios in the bound forms are indicated in yellow for 1:0.25, red for 1:0.5.

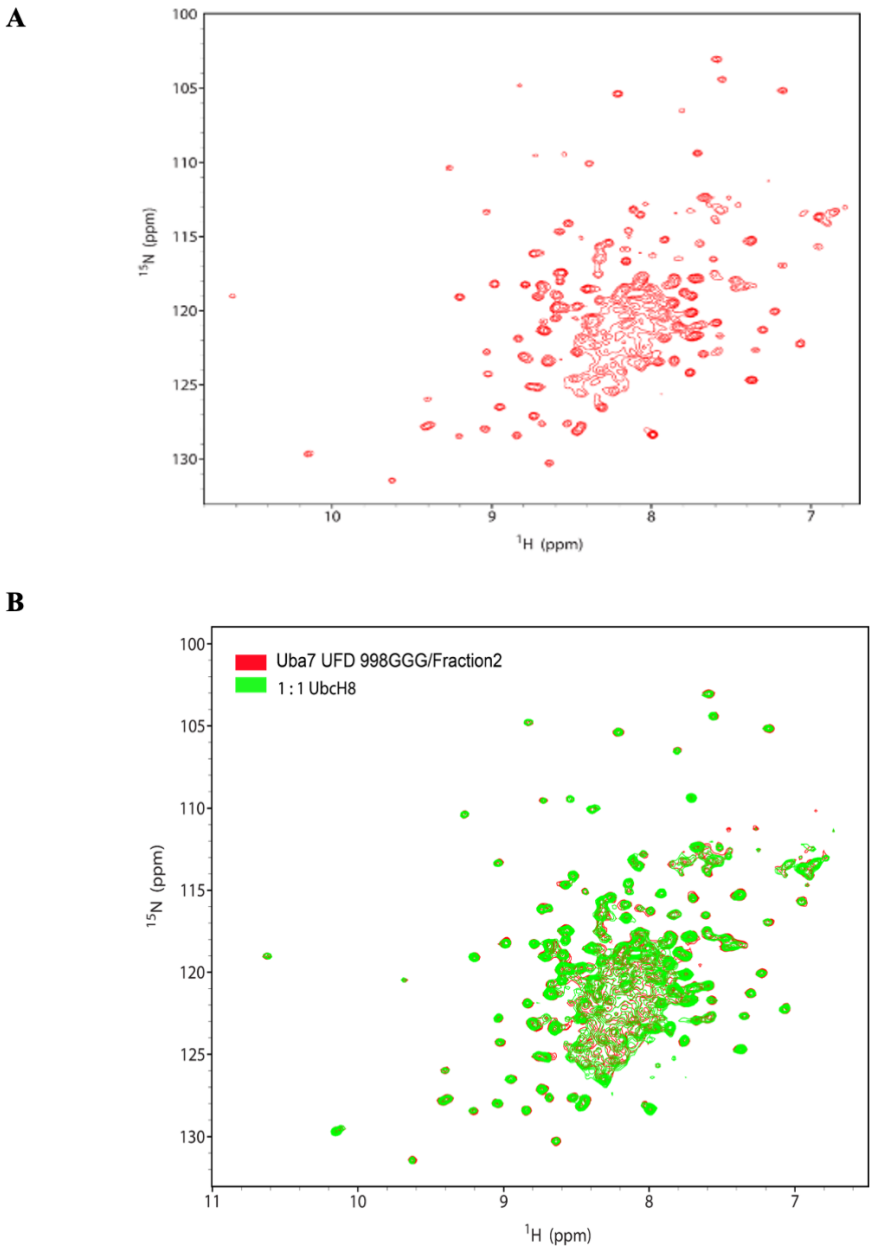

Supplementary Figure 15. 2D NMR analysis of Uba7-UFD 998GGG mutant A. ^{1}H-^{15}N HSQC spectra of free form of 998GGG mutant ^{15}N-GBI-Uba7-UFD B. Superposition of the ^{1}H-^{15}N HSQC spectra of free (red) and 1:1 ratio of UbcH8 bound form of ^{15}N-GBI-Uba7-UFD, 998GGG mutant (Green).

Distance and dihedral restraints	
Short range (|i-j| ≤ 1)	224
Medium range (|i-j| < 5)	319
Long range (|i-j| > 5)	358
Dihedral restraints (φ/ψ)	
Dihedral restrains	153
Total number of restricting constraints	1616
Average RMSD (Å) against the lowest energy model for ordered residues (PSVS)	
Backbone	0.9
All heavy atoms	1.4
RMSD from ideal geometry	
Bond lengths (Å)	0.015
Bond angles (°)	1.4
Consistent violations	
Distance constraints (>0.5 Å)	0
Dihedral angle constraints (>5°)	14.6
Van der Waals constraints (>0.2 Å)	1.8
Ramachandran analysis	
Favoured regions (%)	93.7
Allowed regions (%)	6.2
Generously allowed	0.1
Disallowed	0

Table 1. Restrains and statistics for 20 best solution NMR structures of Uba7-UFD